# An Ultrafast Tunneling Sampler for Atomic-Resolution, High Speed Electronics Measurements

Final Report
May 15, 1992 to September 30, 1995

Offfice of Naval Research
Grant N00014-92-J-1769

G. L. Report No. 5411

*Edward L. Ginzton Laboratory*

STANFORD UNIVERSITY, STANFORD, CALIFORNIA 94305

# An Ultrafast Tunneling Sampler for Atomic-Resolution, High Speed Electronics Measurements

Final Report
May 15, 1992 to September 30, 1995

Offfice of Naval Research
Grant N00014-92-J-1769

G. L. Report No. 5411

Principal Investigator

David M. Bloom

Edward L. Ginzton Laboratory
Stanford University
Stanford, Califronia 94305-4085

# REPORT DOCUMENTATION PAGE

Form Approved
OMB No. 0704-0188



| 1. AGENCY USE ONLY (Leave blank) | 2. REPORT DATE | 3. REPORT TYPE AND DATES COVERED |
|---|---|---|
| | May 1996 | Final 5-15-92 to 9-30-95 |

**4. TITLE AND SUBTITLE**
An Ultrafast Tunneling Sampler for Atomic-Resolution, High-Speed Electronic Measurements

**5. FUNDING NUMBERS**
N00014-92-J-1769

**6. AUTHOR(S)**
B. A. Nechay, A. S. Hou, F. Ho, and D. M. Bloom

**7. PERFORMING ORGANIZATION NAME(S) AND ADDRESS(ES)**
Edward L. Ginzton Laboratory
Stanford University
Stanford, CA 94305-4085

**8. PERFORMING ORGANIZATION REPORT NUMBER**
G.L. 5411

**9. SPONSORING / MONITORING AGENCY NAME(S) AND ADDRESS(ES)**
A. Goodman
Office of Naval Research
800 N. Quincy Street
Code 1114
Arlington, VA 22217-5660

**10. SPONSORING / MONITORING AGENCY REPORT NUMBER**

**11. SUPPLEMENTARY NOTES**
The views, opinions and/or findings contained in this report are those of the authors and should not be construed as an official Department of Defense position, policy or decision unless otherwise documented.

**12a. DISTRIBUTION / AVAILABILITY STATEMENT**
Approved for public release;
distribution unlimited.

**12b. DISTRIBUTION CODE**

**13. ABSTRACT (Maximum 200 words)**

A non-contact probe has been invented and developed for time resolved measurement of electrical waveforms with features as fast as one picosecond. The technique is based on atomic force microscopy modified for electrical sampling. Two generations of probe heads were designed, built, and tested. The fundamental limits of the system, including spatial, temporal, and voltage resolution, have been investigated. State-of-the-art integrated circuits from Intel and National Semiconductor were tested with nanosecond resolution to show that the instrument has potential industrial application. U.S. Patents 5,381,101 and 5,488,305 were granted to Stanford University and licensed to industry. A GaAs nonlinear transmission line was monolithically integrated with a specially designed high speed cantilever and used to probe transients less than one picosecond in duration. Harmonic mixing frequencies as high as 333 GHz were measured.

| 14. SUBJECT TERMS | 15. NUMBER OF PAGES |
|---|---|
| picosecond, nonlinear transmission line, atomic force microscope (AFM), voltage probe, sampling, harmonic mixing, integrated circuit testing, micro-electro-mechanical systems (MEMS), gallium arsenide | 44 |
| | 16. PRICE CODE: NTIS only |

| 17. SECURITY CLASSIFICATION OF REPORT | 18. SECURITY CLASSIFICATION OF THIS PAGE | 19. SECURITY CLASSIFICATION OF ABSTRACT | 20. LIMITATION OF ABSTRACT |
|---|---|---|---|
| Unclassified | Unclassified | Unclassified | SAR |

## 1. Principal Accomplishments

The main achievements of this project have been the following:

- A non-contact probe has been invented for measuring ultrafast time-resolved voltage waveforms on circuits. The technique is based on scanning force microscopy. Traditional measurements of electrical properties using microfabricated force-sensing cantilevers were restricted to the DC-kHz range by the slow cantilever mechanical response. What is new here is the use of the square-law Coulomb interaction between the tip and sample to perform high-speed electrical mixing and equivalent-time sampling. Basic proof-of-principle experiments were conducted to demonstrate the concept.

- U.S. Patent No. 5,381,101, "System and Method of Measuring High-Speed Electrical Waveforms using Force Microscopy and Offset Sampling Frequencies," issued on January 10, 1995, and U.S. Patent No. 5,488,305, "System and Method for High-Speed Potentiometry using Scanning Probe Microscope," issued on January 30, 1996.

- The fundamental limits of the technique, including spatial, temporal, and voltage resolution have been investigated. Improved analytical electrostatic models of the tip and sample are proposed, with a goal towards better understanding of the factors which influence spatial resolution. A circuit model is developed, and expressions are derived for temporal and voltage resolution.

- Two generations of AFM probe heads were designed and built. These designs are tailored for the specific requirements and constraints associated with integrated circuit probing. The necessary electronics for piezo-control, optical detection, and timebase were constructed.

- State-of-the-art integrated circuits, including those from Intel and National Semiconductor, were tested with nanosecond resolution, showing that the probe has promise for making useful measurements of waveform voltage and timing.

- A high-speed transmission line was integrated with a $Si_3N_4$ cantilever and a metallic Spindt tip on a GaAs substrate. The process is developed to be compatible with future integration with picosecond or subpicosecond nonlinear transmission line circuits. A

hybrid chip assembly employing the high-speed cantilever probe was used to make measurements with 5-picosecond time resolution (70 GHz bandwidth).

- Microwave phase measurements were performed using these high-speed cantilever probes showing that the measured phase shift is equal to the applied phase shift, with a phase stability of approximately 0.2 degrees for a 8 GHz source frequency.

- A nonlinear transmission line (NLTL) circuit was monolithically integrated with a specially designed high-speed cantilever. A novel design was developed for the transmission line on the cantilever to allow for a 50-Ohm characteristic impedance. This probe was then used to measure voltage transients as fast as 1 ps, and harmonic mixing frequencies as high as 333 GHz. These are the fastest voltage measurements ever performed using a scanning probe technique.

- A high speed scanning electrical sampler was developed using the AFM in contact mode. Measurements using this probe revealed a 180 ps temporal resolution and 800 $nV/\sqrt{Hz}$ voltage sensitivity.

- A piezoresistive GaAs cantilever was designed, fabricated and characterised. Such a piezoresistive cantilever deflection detection technique avoids the need for optical deflection sensing.

## 2. Motivation

In the last few decades, advances in semiconductor devices and circuits have proceeded at an astounding rate, particularly in the areas of device speed and miniaturization. Indeed, standard transistors used in the semiconductor industry currently have risetimes as fast as 100 ps and minimum linewidths which range around 0.35 μm and expect to reach 0.25 μm by the turn of the century. Up to now, device speeds and dimensions have followed a fairly well defined path of progress, as shown in Fig. 1. This became known as Moore's Law based on the predictions of Gordon Moore of Intel Corp., who surmised that technical progress would make it economical for semiconductor chips to double their transistor density every 18 months. This technical progress was mainly limited by lithographic considerations in which device response followed simple scaling laws with respect to minimum transistor dimensions and these minimum dimensions were progressively decreased based on available lithographic technologies.

These scaling laws are starting to reach their lower limit. Advanced devices are being researched which have linewidths reaching below 0.1 μm and cut-off frequencies in the hundreds of GHz. These devices are approaching limitations in speed and size due to intrinsic material and electrical properties. In such regimes, various physical considerations must be taken into account which include, among others, the quantum mechanical behavior of the electrons and the effects of non-equilibrium or hot-electron transport.

In order to continue developing faster devices and circuits, their high-speed behavior must be well understood and characterized. To achieve this, voltage probing techniques must be used which have measurement bandwidths beyond the transistor cut-off frequencies and lateral resolution small enough to probe within the tenth micron dimensions of these transistors. Unfortunately, the progress in device miniaturisation and speed has outpaced that in measurement technology. Therefore, no voltage probing technique currently exists which has both sufficient temporal resolution and sufficient lateral resolution to properly characterize these fastest devices. Indeed, the high-frequency cut-off behavior of the advanced research devices reported in the literature has been largely extrapolated from available measurement techniques which only go out to about 100 GHz bandwidth.

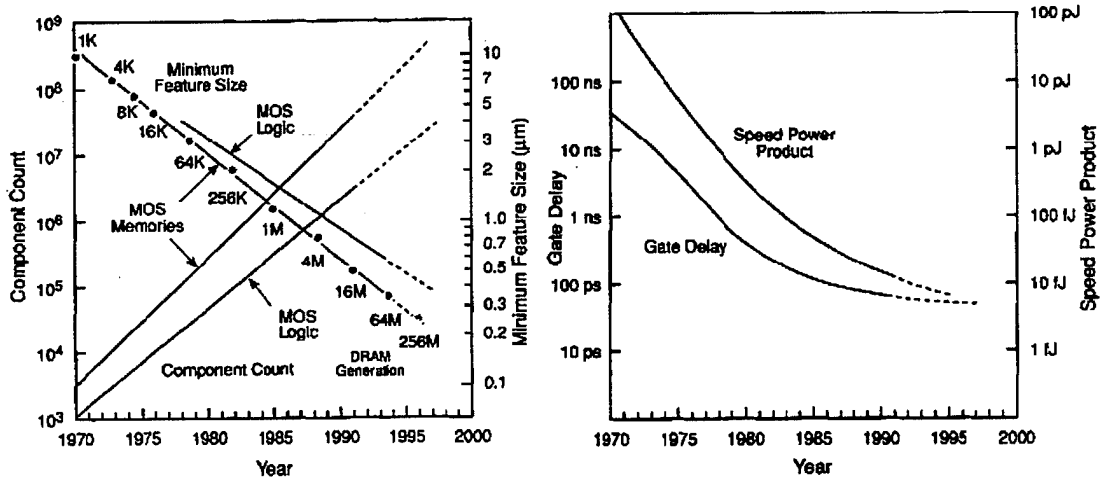


Figure 1. Trends in device size and speed in commercial ICs [1].

This project involved the development of a measurement technique which is capable of probing voltages on devices and circuits with nanometer scale lateral resolution and which has demonstrated temporal resolution as fast as 1 ps, with measured frequencies as high as 333 GHz. These capabilities are accomplished through the combination of nanometer scale probing capabilities of scanning force microscopes (SFM) with high-speed sampling

concepts explored in this research group. The fastest results also combine the high-speed capabilities of the nonlinear transmission line (NLTL) circuit [2], which has proven capable of generating voltage transients as fast as 480 fs[3].

## 3. Scanning Probe Microscopes

Scanning probe microscopes (SPM's) first sprang forth from the Nobel Prize winning invention of the scanning tunnelling microscope (STM) [4] in 1982. Since then, scanning probe systems have developed rapidly into a family of instruments with widespread scientific and commercial applications.

The common thread among all scanning probe microscopes is their use of a sharp tip which can be scanned over a surface and used to measure various physical phenomena. In scanning tunnelling microscopy, for example, the tip is an atomically sharp conducting tip which is positioned to within a few Angstroms of the surface under test. When a voltage is applied to the STM tip, a small tunnelling current arises (typically a few nA) which depends on the local density of electron energy states in the outermost atoms of the surface and tip. This tunnelling current is, therefore, extremely sensitive to the gap between the tip and the sample. Indeed, in general, it can be approximated that each additional Angstrom change in gap distance reduces the tunnelling current by a factor of 10. As the STM tip is scanned over the surface, this gap distance can be kept constant by using the tunnelling current as a feedback parameter. This feedback signal can then be used to map out the topography of the surface atoms.

Another, more versatile, scanning probe technique is the atomic force microscope (AFM), as shown in Fig. 2, which was first invented in 1986 by Binnig, Quate and Gerber [5]. The AFM consists of an atomically sharp tip connected at the end of a flexible cantilever. As the tip is scanned over the surface, atomic forces due to the surface atoms push against the tip and deflect the cantilever. This deflection can be detected via a CW laser which reflects off of a flat region of the cantilever onto a position-sensitive detector. The voltage from this detector can then be used to map out the topography of the sample surface. Alternatively, the cantilever deflection can be kept fixed via a feedback mechanism which controls the sample height with a piezoelectric stack. This feedback signal can then be used to map out the topography.

Scanning Force Microscopes in general are based on the atomic force microscope but are not limited to measurement of atomic forces alone. For example, SFMs that use magnetic tips can map out the magnetostatic forces across the surface of a sample. Electric Force Microscopes, which are particularly relevant to this thesis, use a conductive tip to map

out the electric forces across the surface of a sample in order to gather information about surface voltage, capacitance and charge.

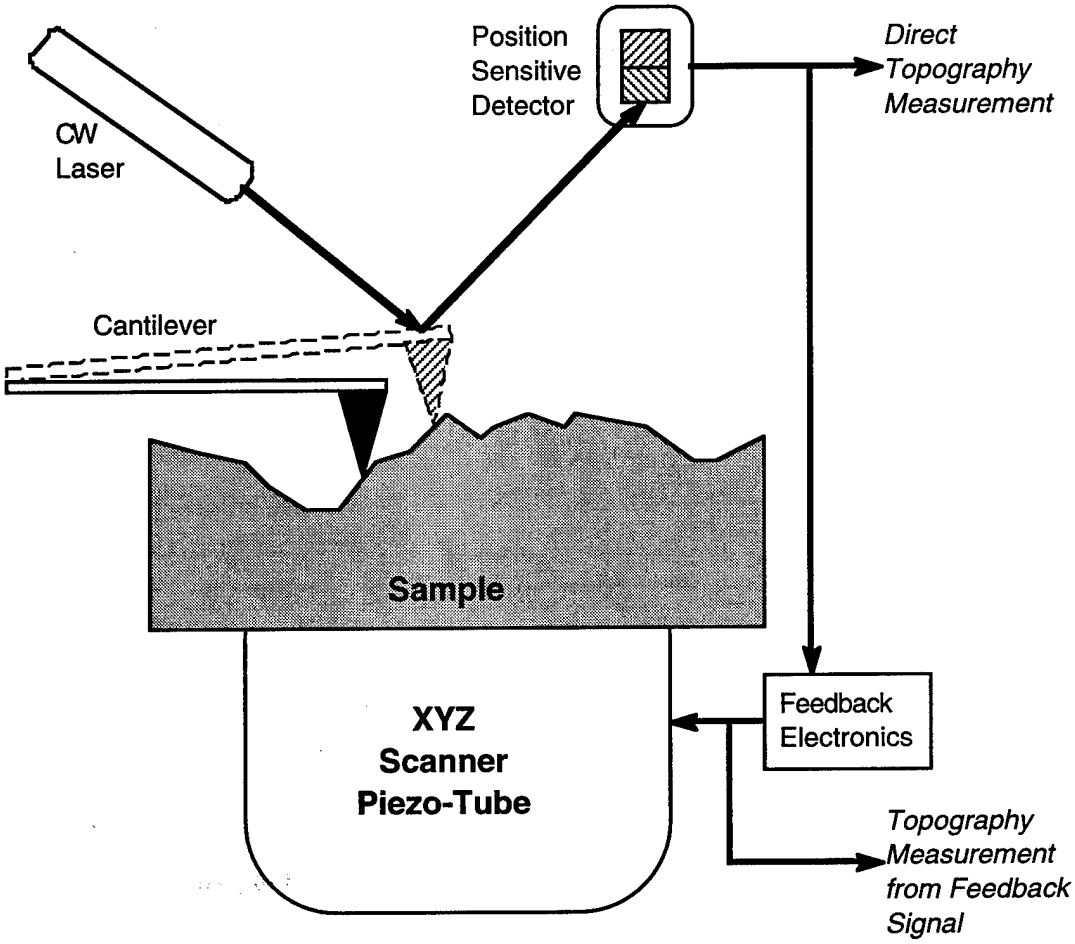


Figure 2. Atomic force microscope.

## 4. High-Frequency Electric Force Measurements with an AFM Voltage Probe

### 4.1 Physical Source of Electric Force Signal

Although the mechanical response of AFM cantilevers are generally limited to a few tens of kHz, the AFM voltage probe has been able to probe MHz signals on commercial ICs and to measure frequency components in MMICs as high as 333 GHz, with corresponding time resolutions as fast as 1 picosecond. The physics behind this technique

involves the use of the voltage squared dependence of the capacitive force between a conductive tip and sample to do harmonic mixing and equivalent time sampling.

Specifically, as shown in Fig. 3, if a conductive AFM tip is suspended above a conductive or semiconductive sample, and a voltage is applied between the tip and the sample, then forces arise which act on the tip in response to this applied voltage. This situation can be modelled as a parallel plate capacitor, with the tip acting as the top plate and the sample acting as the bottom plate.

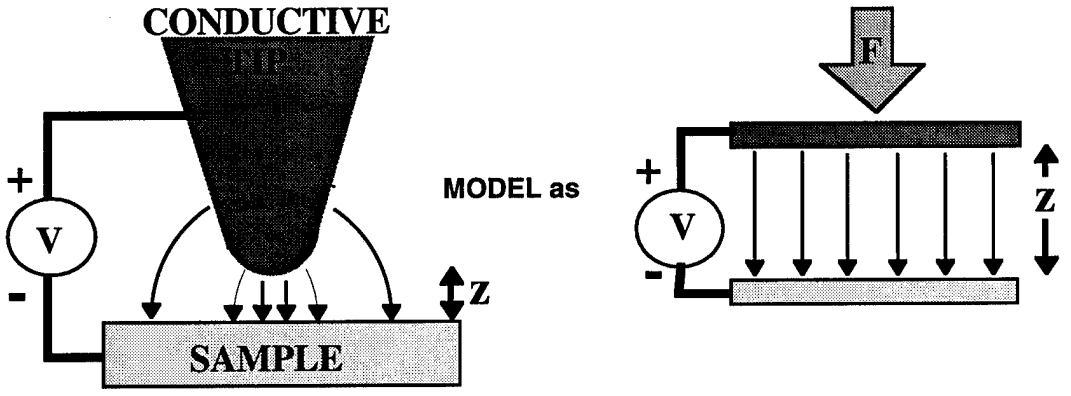


Figure 3. Non-contact conductive tip modelled as a parallel-plate capacitor.

To calculate the force on the tip, one must consider the potential energy of the system and calculate the force from the familiar formula:

$$F = -\frac{\partial U_{tot}}{\partial z} \tag{1}$$

where z is the vertical direction of motion in this case and $U_{tot}$ is the total system electrical potential energy associated with moving the tip in the z direction. Only electrical energy terms are considered since it is the electrical forces due to the applied voltage which are to be calculated. The other force contributions, such as the restoring force of the cantilever and the negligible contributions of gravity, among others, act to cancel out this force at equilibrium.

In order to properly take into account all potential energy contributions for the system electrical potential energy $U_{tot}$, consider that the tip is moved down by an amount dz while keeping the tip-to-sample voltage V fixed. When the tip is moved down by dz, the

capacitance of the tip and therefore the charge on the tip and the electric field between the tip and sample changes. The potential energy of the stored electric field in the tip capacitor is:

$$U_{tip} = \frac{1}{2}\frac{Q_{tip}^2}{C_{tip}} \tag{2}$$

where both $Q_{tip}$ and $C_{tip}$ vary with z. Furthermore, since there is a change in the charge on the tip, these charges have to come from somewhere. In this case, they are drawn from a battery or voltage source, which acts as a reservoir of charge and can be modelled as a large capacitor whose loss of this charge makes only a negligible change in its voltage. The potential energy of the battery can be calculated as:

$$U_{bat} = \frac{1}{2}\frac{Q_{bat}^2}{C_{bat}} \tag{3}$$

where only $Q_{bat}$ is now dependent on z and $dQ_{bat} = -dQ_{tip}$ due to conservation of charge. The net electrical force on the tip can then be calculated as follows:

$$\begin{aligned} F &= -\frac{\partial U_{tot}}{\partial z} \\ &= -\left(\frac{\partial U_{bat}}{\partial z} + \frac{\partial U_{tip}}{\partial z}\right) \\ &= -\left(\frac{Q_{bat}}{C_{bat}}\frac{\partial Q_{bat}}{\partial z} + \frac{Q_{tip}}{C_{tip}}\frac{\partial Q_{tip}}{\partial z} - \frac{1}{2}\frac{Q_{tip}^2}{C_{tip}^2}\frac{\partial C_{tip}}{\partial z}\right) \\ &= -\left(\left(\frac{Q_{tip}}{C_{tip}} - \frac{Q_{bat}}{C_{bat}}\right)\frac{\partial Q_{tip}}{\partial z} - \frac{1}{2}\frac{Q_{tip}^2}{C_{tip}^2}\frac{\partial C_{tip}}{\partial z}\right) \end{aligned} \tag{4}$$

Now, since the tip to sample voltage V is equal to the battery voltage, so that

$$V = \frac{Q_{tip}}{C_{tip}} = \frac{Q_{bat}}{C_{bat}} \tag{5}$$

then the first force term cancels and the force simplifies to:

$$F = \frac{1}{2}\frac{\partial C_{tip}}{\partial z}V^2 \tag{6}$$

Since capacitance decreases as the capacitor electrodes are moved farther away, this term is negative and, therefore, the force is an attractive one. In the parallel plate capacitor case, the capacitance is equal to $\varepsilon_0 A/z$ and the force is then:

$$F = -\frac{\varepsilon_0 A}{2z^2}V^2 \tag{7}$$

The significant thing to note here is that the electrical force is proportional to the square of the applied voltage between the tip and the sample. This square-law dependence is very important since it is the mathematical relationship which allows the use of harmonic mixing and equivalent-time sampling, as described in the next section, which gives the ultrafast time resolution.

### 4.2 High Frequency Electrical Mixing

As shown in the last section, the attractive electrical force between the tip and the sample varies as the square of the tip-sample voltage V:

$$F = \frac{1}{2}\frac{\partial C_{tip}}{\partial z}V^2 \tag{8}$$

where $V = V_{tip} - V_{sample}$. Carrying out the square term, one gets:

$$F = \frac{1}{2}\frac{\partial C_{tip}}{\partial z}(V_{tip}^2 - 2V_{tip}V_{sample} + V_{sample}^2) \tag{9}$$

If $V_{tip}$ and $V_{sample}$ are both high frequency signals with frequency components at DC and at frequencies above the cantilever mechanical response cut-off frequency, or resonance frequency $f_{res}$, then the only force terms which are within the cantilever response are DC terms, which are ignored, and the offset frequency signals from the $V_{tip}V_{sample}$ term. This term thus allows one to do harmonic mixing and equivalent-time sampling, which are used to measure voltage waveforms much faster than $f_{res}$.

#### 4.2.1 Mixing

Assume that the signal on the tip and sample are:

$$V_{tip} = V_{AC,tip} \cos(\omega_t t) \tag{10}$$

$$V_{sample} = V_{AC,sample} \cos(\omega_s t) + V_{DC} \tag{11}$$

then the force on the tip becomes ( setting $K = 1/2\ \delta C_{tip}/\delta z$ ):

$$\begin{aligned} F &= K\,(V_{tip}^2 - 2\,V_{tip}\,V_{sample} + V_{sample}^2) \\ &= K\,[\,V_{AC,tip}^2 \cos^2(\omega_t t) - 2V_{AC,tip}\,V_{AC,sample} \cos(\omega_t t)\cos(\omega_s t) \\ &\quad - 2V_{AC,tip}\,V_{DC} \cos(\omega_t t) + V_{AC,sample}^2 \cos^2(\omega_s t) + V_{DC}^2 \\ &\quad + 2V_{AC,sample}\,V_{DC} \cos(\omega_s t)\,] \end{aligned} \tag{12}$$

Using the trigonometric identities :

$$\cos(\omega_t t)\cos(\omega_s t) = 1/2\,[\cos((\omega_t + \omega_s)t) + \cos((\omega_t - \omega_s)t)]$$
$$\cos^2(\omega t) = 1/2\,[1 + \cos(2\omega t)]$$

and grouping like-frequency terms together, one gets:

$$\begin{aligned} F = K/2\ \{[\,&V_{AC,tip}^2 + V_{AC,sample}^2 + 2V_{DC}^2] && \textit{DC terms} \\ +\ &[4V_{AC,sample}\,V_{DC}\,\underline{\cos(\omega_s t)} - 4V_{AC,tip}\,V_{DC}\,\underline{\cos(\omega_t t)}] && \textit{1st harmonic} \\ +\ &[V_{AC,tip}^2\underline{\cos(2\omega_t t)} + V_{AC,sample}^2\underline{\cos(2\omega_s t)}] && \textit{2nd harmonic} \\ -\ &2V_{AC,tip}\,V_{AC,sample}\,\underline{\cos((\omega_t + \omega_s)t)} && \textit{mixed term} \\ -\ &2V_{AC,tip}\,V_{AC,sample}\,\underline{\cos((\omega_t - \omega_s)t)}\ \} && \textit{mixed term} \end{aligned} \tag{13}$$

When $\omega_t$ and $\omega_s$ are above the cantilever resonance frequency $\omega_0$ but $\Delta\omega = \omega_t - \omega_s$ is below $\omega_0$ then the cantilever can only respond to the DC terms, which are generally ignored, and to the slow difference frequency terms. The actual cantilever deflection which can then be measured is:

$$\text{deflection} = F/k = -K\,V_{AC,tip}\,V_{AC,sample} \cos((\omega_t - \omega_s)t) \tag{14}$$

If we apply a known signal to the tip at a frequency close to the sample frequency, then we can determine the unknown sample signal by measuring the frequency and amplitude of the vibrating cantilever.

### 4.2.2 Harmonic Mixing

This technique can be extended to signals that have numerous harmonics of $\omega_t$ and $\omega_s$ (in other words, signals that repeat at these frequencies but are arbitrary waveforms, not just sinusoids). In this case, the most useful signal to apply to the tip is a set of sampling pulses at a slightly lower repetition frequency than the sample repetition rate. This scenario is shown in Fig. 4(a-d). Here, the sample signal repeats at a frequency $f_s$ and has a spectrum (Fig. 4(a)) which dies off at higher harmonics. The tip signal is a train of sampling pulses at a repetition frequency $f_s - \Delta f$ which, in the frequency domain, give rise to a range of harmonics with roughly equal amplitude. In the ideal case, the pulse width would be zero, giving rise to a frequency domain signal with equal amplitude harmonics stretching out to $+/- \infty$. In the real case, the pulse width of the tip signal is finite, leading to a rolloff of the amplitude of the harmonics at high frequencies (Fig. 4(b)).

Multiplication in the time domain corresponds to convolution in the frequency domain:

If $$c(t) = a(t)\, b(t)$$

then

$$C(f) = A(f) * B(f) = \int_{-\infty}^{\infty} A(f)B(f' - f)df \qquad (15)$$

Therefore, the time-domain multiplication of the tip and sample signals of the example give rise to a force spectrum shown in Fig. 4(c), which shows a frequency-compressed version of the sample signal spectrum repeated at $f_s$ intervals. Since the cantilever can only respond to the slow frequencies, then the spectrum of the measured cantilever reflection, shown in Fig. 4(d), is a low-pass-filtered version of the force spectrum. As can be seen, this is an exact mapping of the original sample signal onto a slower frequency $\Delta f$, with a corresponding "stretching" of the sampled signal in the time domain by a factor of $f_s/\Delta f$. The only requirement here is that the rolloff frequency of the tip signal be higher than the highest significant frequency in the sample voltage spectrum. Otherwise, the final sampled signal will not have enough time resolution to show the finer features of the sample voltage waveform. Indeed, the measurement bandwidth of this system can be quoted as the 3 dB bandwidth of the sampling pulses, namely, the frequency at which the spectrum reduces by a factor of $1 / \sqrt{2}$ of its DC value. For a gaussian pulse with a full-width at half-maximum (FWHM) of $\tau$, the 3 dB bandwidth is $f_{3dB} = 0.312 / \tau$.

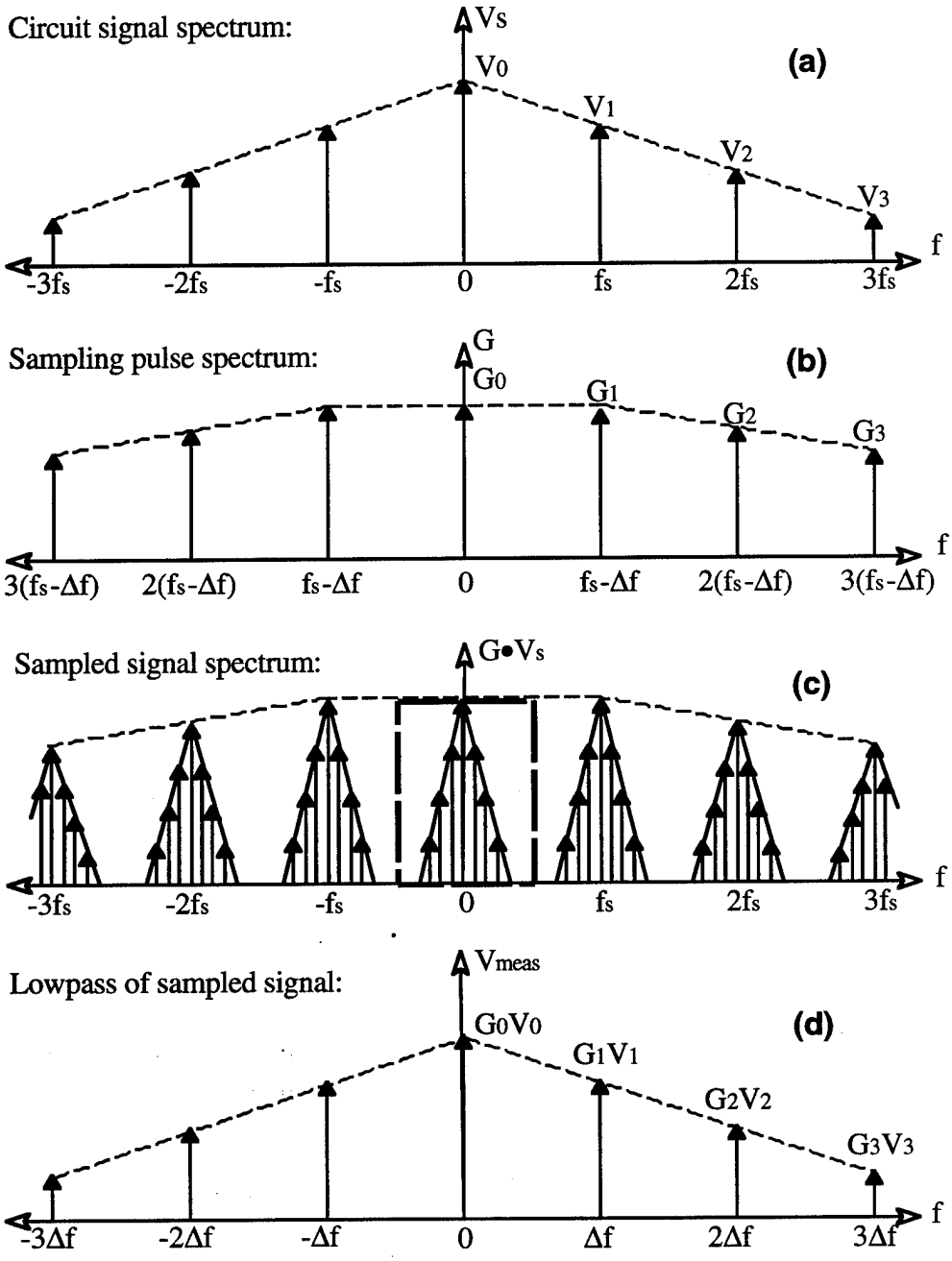


Figure 4. Harmonic mixing.

### 4.2.3 Equivalent Time Sampling

These concepts might be viewed more easily in the time domain as so called "equivalent-time sampling." This sampling method forms the basis behind almost all time-resolved measurements of high speed signals, such as those used in high speed sampling

oscilloscopes. In equivalent-time sampling, a set of sampling pulses essentially take "snapshots" at different points in each cycle of the repetitive voltage waveform to be measured. This can be thought of as being analogous to a strobe lamp taking snapshots of a fast repetitive event, such as falling water droplets, to capture their movement in slow-motion. These "snapshots" of the repetitive voltage waveform are usually accomplished through techniques which cause the sampling pulses to open a measurement window. These include methods which make use of photoconductive gaps and those which use transistors acting as fast switches to open a gate through which a voltage measurement is taken. The term "sampling" most commonly refers to these sorts of methods of gating the measured signal. In the case of the AFM Voltage Probe, however, the "snapshots" of the voltage waveform are accomplished through the use of nonlinearities in the voltage dependence of the measured signal to mix the sampling and sample signal. The term "sampling" will continue to be used within this report, however, since it best represents most of the high-speed measurement concepts employed by the AFM Voltage Probe.

Figure 5 shows these equivalent-time sampling concepts for the measurement scenario employed by this system. Here, the signal under test repeats at a frequency $f_s$, which can be as high as tens of GHz. To sample this fast signal, a set of sampling pulses is applied to the tip at a slightly lower frequency $f_s - \Delta f$ so that the sampling pulses "walk-through" the signal waveform. The force acting on the tip then has terms which vary as the product of these two signals $V_{tip}V_{sample}$. This results in force components which vary as a train of pulses whose amplitudes trace out the original signal waveform at a repetition rate of $\Delta f$. Since the cantilever can only respond to low frequency components of the force, it simply deflects with an amplitude proportional to the slow running average of the force signal, which simply follows the envelope of these pulses.

Mathematically, this results in a cantilever deflection:

$$\Delta z(t) = -\frac{1}{k}\frac{\partial C_{tip}}{\partial z}\frac{\tau}{T_s}[V_p g(\frac{\Delta f}{f_s}t) * V_{sample}(\frac{\Delta f}{f_s}t)] \tag{16}$$

where k is the spring constant of the cantilever, $\tau$ is the sampling pulse width, Ts=1/fs, "*" indicates a convolution operation, Vp is the sampling pulse amplitude and g(t) is the sampling pulse shape. For sampling pulse widths shorter than the smallest significant temporal feature of the signal under test, this can be approximated as:

$$\Delta z(t) = -\frac{1}{k}\frac{\partial C_{tip}}{\partial z}\frac{\tau}{T_s}V_p V_{sample}(\frac{\Delta f}{f_s}t) \tag{17}$$

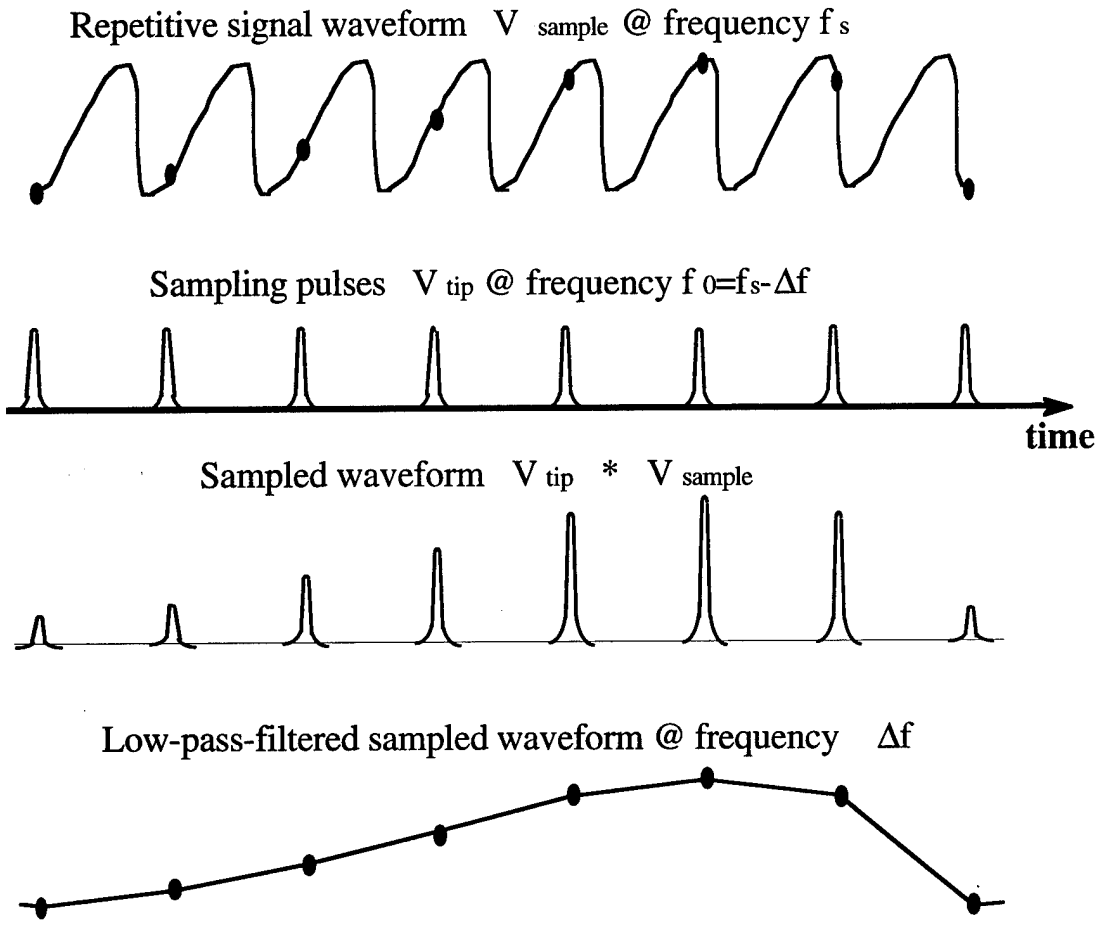


Figure 5. Equivalent time sampling.

In this way, the measured cantilever deflection is proportional to the time-expanded version of the signal waveform, with an expansion factor of $f_s/\Delta f$ .

There are a few things to note about this system. Firstly, the time-width of the sampling pulses sets the limit of the time resolution of the system (which, in this case, can be as fast as 1 ps). This is equivalent to the limitation of the 3 dB bandwidth of the sampling pulses in the frequency domain, as explained in the last section. Also, the offset frequency should be small enough so that the sampling steps are short, which can be a consideration when measuring voltage waveforms with repetition frequencies below about 100 kHz. The sampling steps can be calculated as $(\Delta f/f_s)T_s$ where $T_s$ is the time period of the repetitive signal under test. Finally, if both of these conditions are met, then this technique can accurately measure signals with bandwidths in the hundreds of GHz range, limited only by the sampling pulse width.

## 5. Ultimate Time Resolution

As was mentioned earlier, the temporal resolution of this measurement system is mainly limited by the available sampling signal source speed. However, the sampling probe itself presents a load which, though very small, ultimately limits the speed of the sampling signal which can get to the tip, independent of the signal source. To understand the nature of the sampling probe load to the source, it is useful to examine the equivalent circuit model, as shown in Fig. 6. In this model, $R_{pulse}$ and $R_{circ}$ represent the output impedances of the probe and sample signal sources, respectively; $C_{tip}$ represents the tip-to-sample capacitance; $C_{gnd}$ is the ground coupling capacitance; and Lgnd is the inductive external ground connection.

From this equivalent circuit, an equivalent series RC load can be calculated, which gives rise to an RC time constant:

$$\tau_{RC} = (R_{pulse} + R_{circ})\, C_{tip}\, C_{gnd} / (C_{tip} + C_{gnd}) \qquad (18)$$

and corresponds to a 3 dB cutoff frequency of $1 / 2\pi\tau_{RC}$. This is the frequency at which the voltage across the tip drops by $1 / \sqrt{2}$ and represents the intrinsic speed limit to the AFM voltage sampling technique. If one assumes $C_{tip} \sim 0.1$ fF $<< C_{gnd}$ and $R_{pulse} \sim R_{circ} \sim 50\Omega$, then one can calculate the 3 dB frequency as 16 THz. The actual tip capacitance might also include additional stray capacitances, but these can be greatly reduced with proper probe design.

## 6. Voltage Resolution

The voltage resolution of this AFM voltage sampling technique is determined by the noise sources within the system. These include:

- Laser Shot Noise: This is due to the statistical arrival of photons on the position sensitive photodetector of the cantilever deflection sensor, giving rise to a noise in detector voltage.

- Laser Intensity Noise: This is caused by other sources of noise in the laser diode of the cantilever deflection sensing mechanism. These include spontaneous emission, mode-partition noise, mode-hopping noise and 1/f noise.

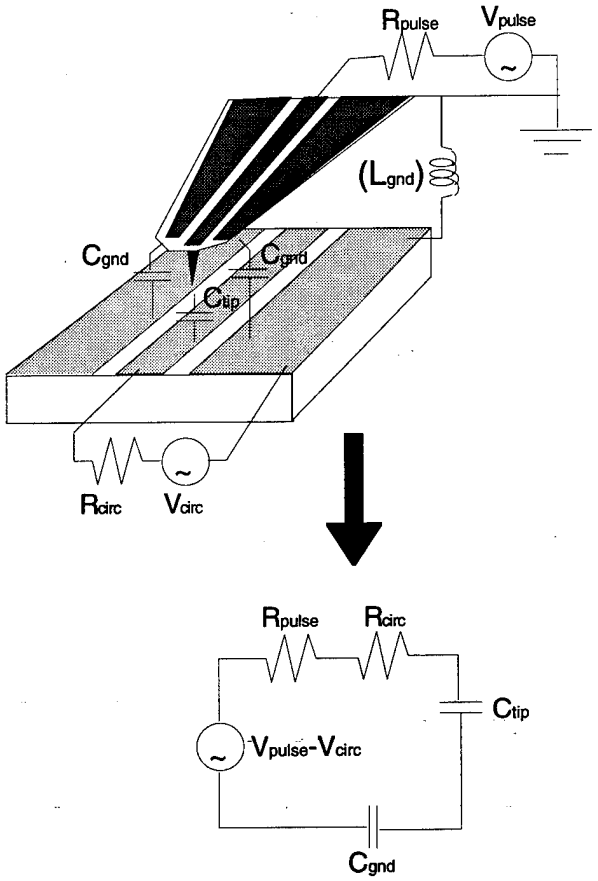


Figure 6. Equivalent circuit model.

- Electrical Noise in the Detection Electronics: This includes electrical noise within the detector itself and in the subsequent signal processing electronics.

- Thermal-Mechanical Noise of the Cantilever: This is the broadband random deflection noise of the cantilever due to its thermal equilibrium with the environment. Specifically, the heated air molecules collide with the cantilever and excite oscillations at a broad frequency range. This thermal-mechanical cantilever noise is by far the largest noise source in the system.

The minimum detectable voltage based on the thermal-mechanical noise of the cantilever, the dominant noise contribution in the measurement system, can be calculated from the following formula:

$$V_{min} = \frac{z^2}{\varepsilon_0 A V_p} \sqrt{\frac{32 k k_B T}{f_0 Q}} \frac{1}{D^{3/2} T_{acq}^{1/2}} \tag{19}$$

where z, A, k, $f_0$ and Q are the flying height, area, spring constant, resonance frequency and Quality-factor of the AFM tip and cantilever; T is the temperature, $k_B$ is Boltzmann's constant, $\varepsilon_0$ is the permittivity of free space; $V_p$ is the probe voltage, D is the duty cycle (probe pulsewidth/repetition time) and $T_{acq}$ is the data acquisition or averaging time. Examples of optimised values for some of these variables for the probes and measurements described in this report are shown in Table 1.

**Table 1 - Typical Probe System Parameters**

| | | |
|---|---|---|
| Tip flying height | z | 100 Å |
| Tip effective area | A | 0.05 $\mu m^2$ |
| Sampling pulse amplitude | $V_p$ | 3 V |
| Duty cycle | D | 0.01 |
| Cantilever spring constant | k | 0.9 N/m |
| Resonance frequency | $f_0$ | 22 kHz |
| Quality factor | Q | 10 |

Using the values of the probe parameters listed in the table, and assuming a total acquisition time of 100 sec and room temperature, the minimum detectable voltage can be calculated as:

$$V_{min} \approx 5 \text{ mV} \qquad \text{for } T_{acq} = 100 \text{ sec} \tag{20}$$

Various methods can be employed to increase the signal to noise ratio of the system and, therefore, lower the minimum detectable voltage. First of all, the thermal-mechanical noise of the cantilever can be reduced by going to lower temperatures, increasing the Q of the cantilever (by using a crystalline material for the body of the cantilever or going into a vacuum environment, for example) or simply by averaging the data over more periods (longer acquisition time). Also, larger-amplitude sampling voltages can be used, tip area increased or flying height decreased in order to increase the signal strength. The duty cycle can also be increased, but this reduces the temporal resolution of the measurement.

There are limitations to how close to the sample the tip can fly. Namely, below a certain height called the "snapping height," the force gradients acting on the tip become

larger than the spring constant of the cantilever. This results in an unstable situation in which the restorative force of the cantilever cannot compensate for force fluctuations, and the tip "snaps" down to the surface. This snapping height is smaller for larger k cantilevers. Therefore, it is generally better for signal-to-noise ratio considerations to use a somewhat higher-k cantilever, assuming that the vibration isolation of the system is good enough to support such a close flying height. Though higher-k cantilevers also have larger thermal-mechanical noise, this is more than compensated for by the increased signal strength due to smaller allowable tip flying height. The lower limitation on the tip flying height, and therefore the upper limitation on k, results when the flying height is no longer large compared to the cantilever deflection amplitude due to electric force signal, since non-linear second-order effects then start coming into play.

## 7. Lateral Resolution

The lateral resolution of the AFM Voltage Probe is mainly determined by the electric field distribution between the sample and the tip or signal line of the AFM cantilever, as shown in Fig. 7. For tall and sharp tips close to the sample, the vertical electric force contribution on the bottom part of the tip is generally much greater than that for the top part of the tip or for the AFM signal line since the electric field strength varies as $1/z^2$. Therefore, the lateral resolution in this case is mainly limited by the tip radius and flying height. For tall 300 Å radius tips at a 100 Å flying height, the lateral resolution might then be estimated to be about 0.1 μm.

However, for duller tips with lower aspect ratios or higher flying heights, the sides of the tip as well as the cantilever signal line can add significant electric force contributions and, therefore, reduce the attainable lateral resolution. The ideal AFM tip would thus be extremely sharp and tall and have vertical sidewalls in order to keep all of the electric force contributions at the tip end.

## 8. Early Proof-of-Principle Experiments

One of the important early proof-of-principle experiments involved the cross-correlation measurement of two pulse trains that were launched onto a coplanar transmission line (CPW) sample, as shown in Fig. 8. The pulse trains were generated by sending amplified sinusoidal signals at 500 MHz and 500 MHz + 10 Hz through step-recovery-diodes (SRD) to generate a train of 100 ps pulses. A gold-coated silicon nitride tip was grounded in this experiment and the electrical force terms which caused the

measured cantilever deflection were due to the $V_{sample}^2$ term of Eq. 9. This is based on the same physical processes as the mixing and equivalent-time sampling methods described in Section 4. The resulting cross-correlation measurements are shown in Fig. 9 showing a 130 ps measured pulsewidth.

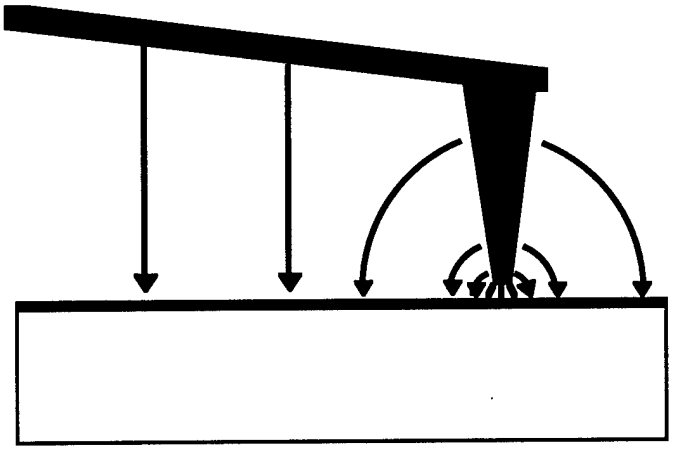

Figure 7. Electric field distributions between tip and sample.

In another early experiment, we used the setup as diagrammed in Fig. 10(a). This experiment varied from the previous one in that the SFM system was used to sample the output of an HP8133A word generator as opposed to another SRD pulse train. The test word consisted of 32 bits, with digital voltage levels of 0 and 3.3 volts. The clock rate was 3.2 GHz, so that the 32-bit pattern repeated at a rate of 100 MHz. A step-recovery diode comb generator was again used to generate a train of 100 ps sampling pulses at the repetition rate of 100 MHz - 100 Hz. The word generator output and the sampling pulses were combined and launched onto a 50 Ω coplanar waveguide (CPW) transmission line on GaAs. The center signal conductor was 15 microns wide. Because there was a 100 Hz frequency offset between the digital data stream and the pulse train, the pulses effectively "walked through" the data, yielding an equivalent-time signal at 100 Hz. In all of our experiments, the IF frequency, 100 Hz in this case, was chosen to be high enough to lie above the 1/f noise of the system yet low enough for all of its relevant harmonics to lie within the flat region of cantilever mechanical response. Figure 10(b) shows that the sampled result agreed very well with the direct output of the HP8133A as measured with a 20 GHz sampling scope.

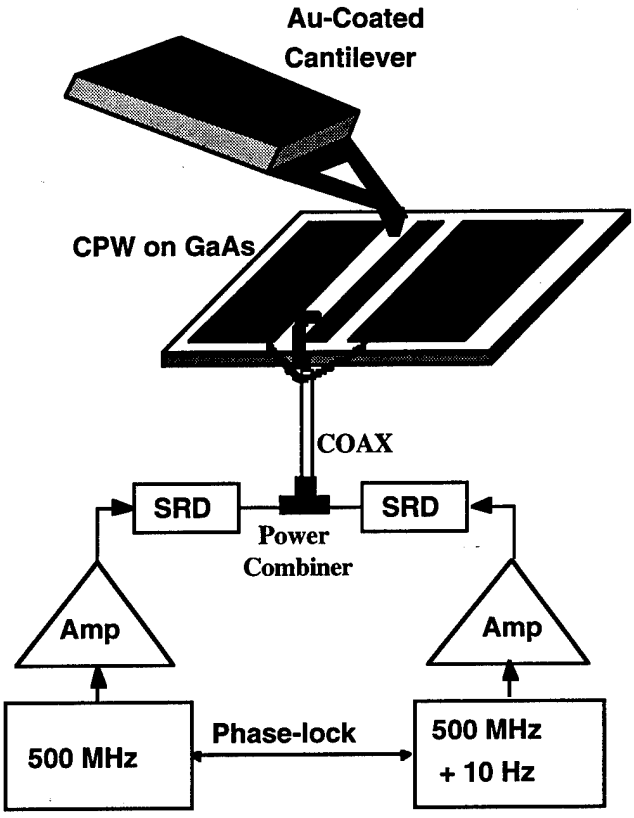


Figure 8. Experimental set-up for pulse cross-correlation experiment.

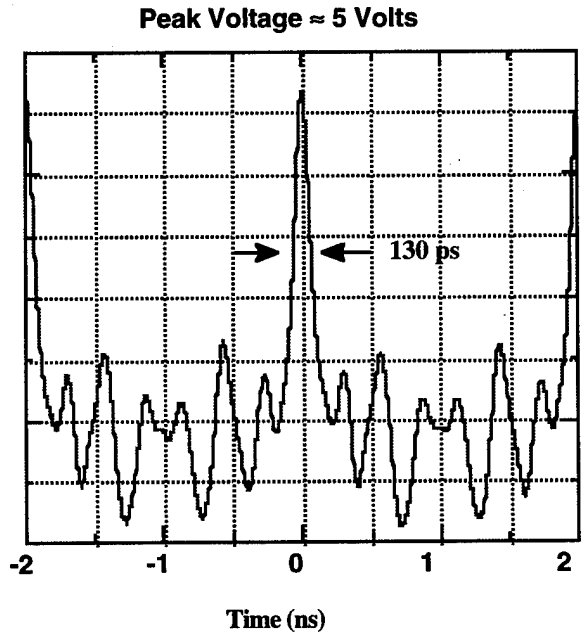


Figure 9. Results of pulse cross-correlation showing 130 ps FWHM.

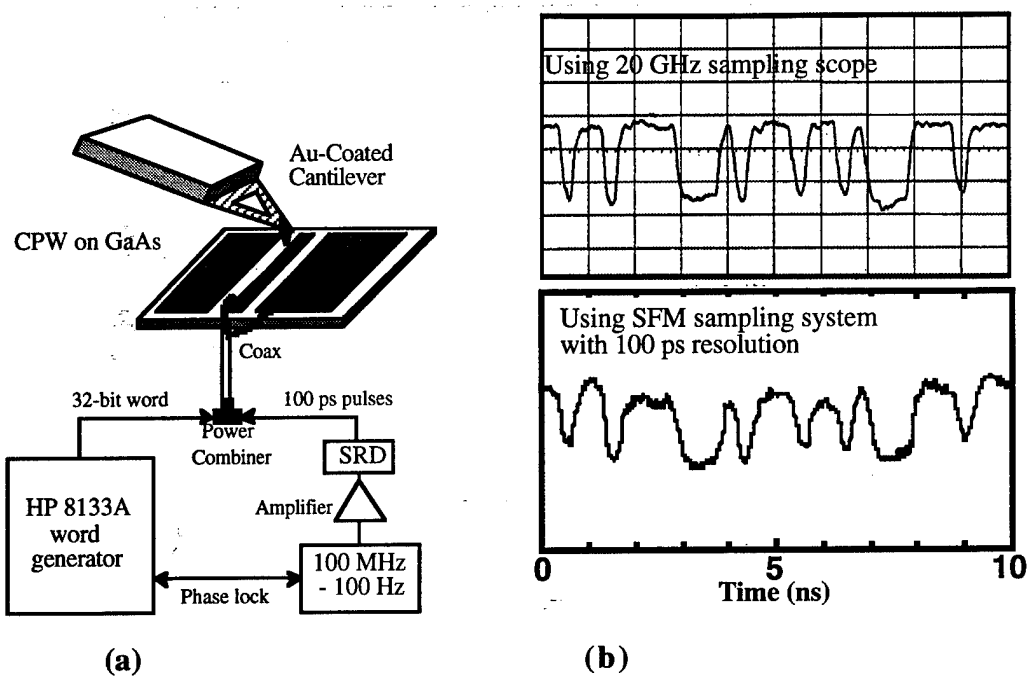


Figure 10. Set-up and measurements of HP8133A generated word.

## 9. Probe Design and Engineering

One of the main goals of designing such an AFM voltage probe was to be able to use it to measure integrated circuits. However, probing integrated circuits places severe mechanical constraints on overall system design. These constraints include the need to be able to probe within the often deep recesses of IC chips to reach a particular signal node. Furthermore, it is preferable to scan the probe tip as opposed to the sample (as is done in most commercial systems) since the sample may be heavy or difficult to move due to attached I/O signal wires or even microwave contact probes. Since our commercial AFM system couldn't meet our needs in this regard, custom AFM probe heads needed to be designed.

In the design of the AFM probe heads, various mechanical considerations needed to be taken into account. First of all, the probe had to be mechanically stable. This involved the suppression of vibration noise and thermal drift. Furthermore, it was preferable to have a flexible modular design for the probe which would allow for the easy replacement of the probe cartridge.

The final generation probe design is shown in Fig. 11(a), with a photo of the probe shown in Fig. 11(b). The cantilever deflection detection is accomplished with an optical detection scheme. This consists of an InGaAlIp, 670 nm, 5 mW laser diode focused

through a mirror onto the cantilever, with the deflected beam bouncing back on the mirror to a position-sensitive photodetector. Clearance was left above the cantilever for a 50X long-working-distance objective lens for optical viewing. This design also incorporates piezoelectric stacks which control the x and y scanning of the head as well as the fine z positioning of the tip. Fig. 11(c) shows a diagram of a chip holder which mounts on the probe head and makes microwave signal and ground connections to the attached microwave cable. The custom AFM cantilever chips are then mounted and wirebonded to their own chip holders. Therefore, this design allows for the easy replacement of the AFM cantilevers.

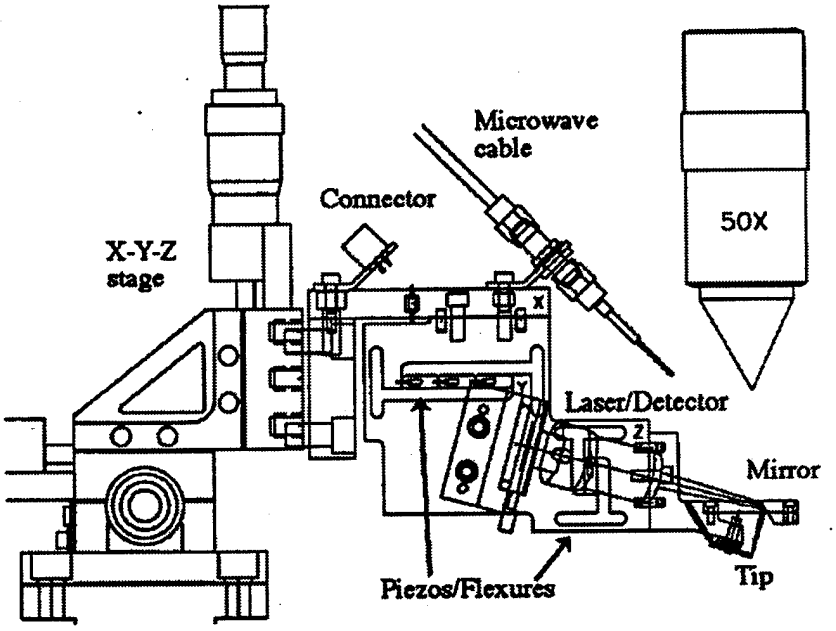


(a)

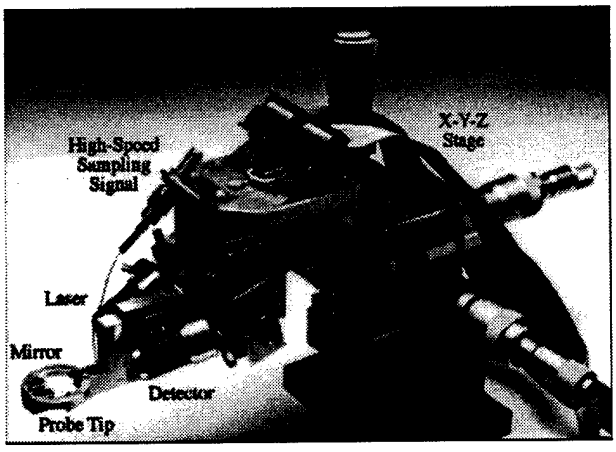


(b)

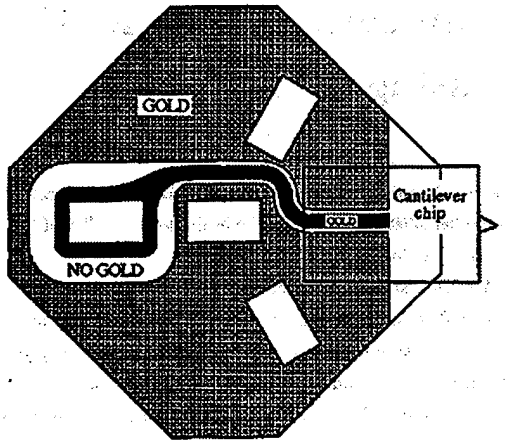


(c)

Figure 11. Second generation AFM probe head (a) design, (b) photo, (c) chip holder.

## 10. Measurements of Integrated Circuits

An early application experiment which demonstrates the advantages and limitations of the measurement technique involved the measurement of voltages at various points of a shift-register chip, as shown in Fig. 12. This circuit had a 1 μm thick passivation layer on top. Nevertheless, the AFM voltage probe was still able to measure the high-frequency signals. The measurements at points 1 through 4 are shown in Fig.13. Here, one can see the data shifting in phase as one proceeds along the points of the shift-register. However, since the tip flying height was at least 1 μm, the stray electric fields contributed much more to signal than in the case of a few hundred Angstrom tip flying height. This meant that the lateral resolution was much worse and that there was considerable overlap of the signal contribution from various measurement points. This can also be seen in the plot, where one can see contributions of signal 1 in the measurements at point 2, etc.

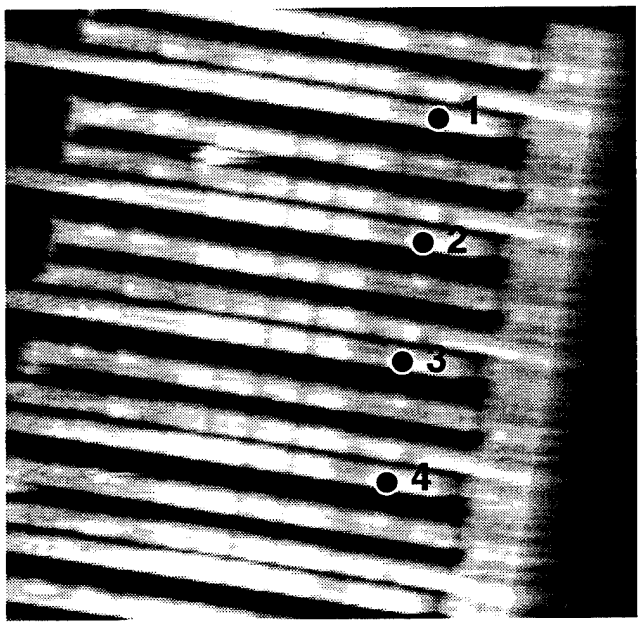


Figure 12. AFM topographical scan of shift register contacts.

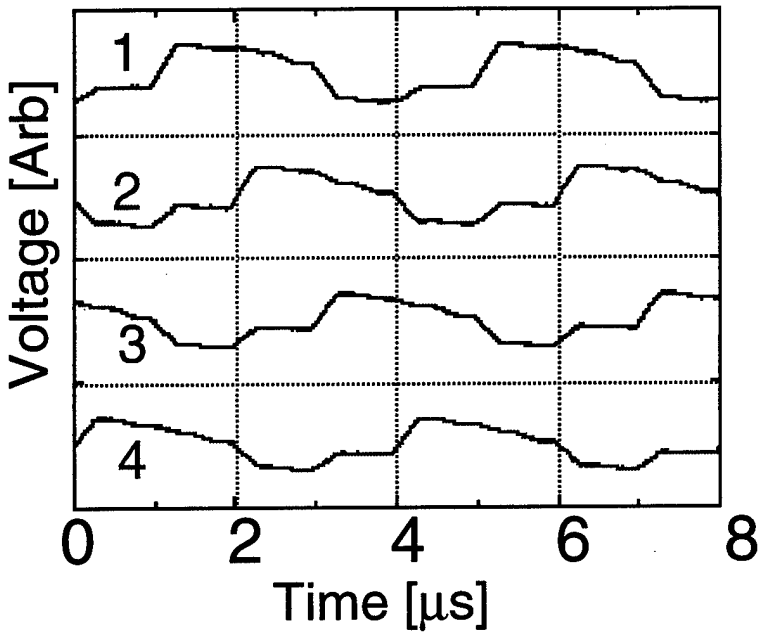


Figure 13. Voltage waveforms on shift register measured by AFM probe.

Figures 14(a) and (b) show measurements of internal voltages on an Intel 80486 microprocessor chip. The chip had been mounted in a inverted-cavity pin-grid-array package and depassivated. Figure 14(a) shows two 20 MHz clock signals of opposite phases. The sampling pulses used were 2 ns wide. Figure 14(b) shows a sampled result of a 2 μs-long test vector that was produced by applying a reset signal to the chip every 20 clock cycles. The bit pattern of zeros and ones can be clearly discerned.

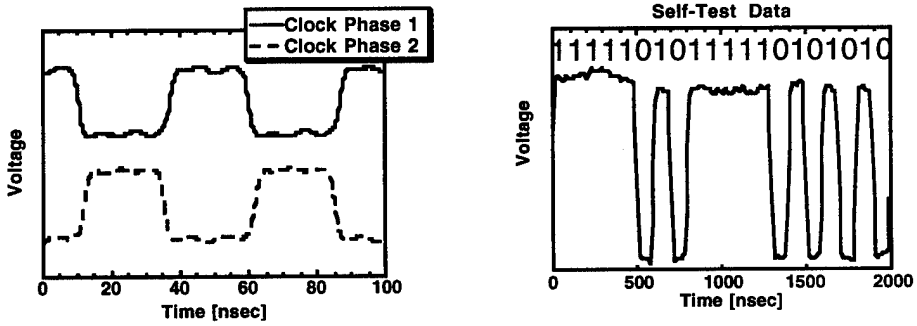


Figure 14. Measurements of an INTEL 80486 microprocessor chip.

Another integrated circuit that was measured is National Semiconductor's AT/LANTIC (AT local area network twisted-pair interface controller) chip. The

AT/LANTIC incorporates a clock-recovery phase-lock loop to synchronise incoming ethernet data, which for this experiment was simulated by test driver circuitry. A challenge in testing the AT/LANTIC was in building the timebase electronics required for generating sampling pulses with proper timing with respect to the chip. Every 25 μs, the test circuitry repeats the data pattern and generates a trigger signal. As shown in Fig. 15, this trigger signal is delayed using a programmable digital delay circuit (based on Analog Devices' AD9501) and used to trigger a pulse generator. With this type of timebase circuit, arbitrary delays as long as several tens of microseconds with a delay resolution of 100 picoseconds are possible. Measured data from the chip are shown in Fig. 16. PHCOMP is an asynchronous digital signal which requires about 250 ns to settle to a valid state. The first complete rising edge of PHCOMP (occurring at t = 330 ns) is found to be significantly longer (15 ns) than subsequent edges (about 6 ns). The amount of edge broadening is a measure of the jitter in AT/LANTIC's phase-lock loop and also a function of the averaging time for the measurement. In comparison, a second, synchronous signal from the chip (DMUX) showed no significant difference in edge speeds from edge to edge. These results demonstrate the usefulness of the probe system for making precise timing and delay measurements. Also, the long loop times in this experiment are closer to those typically used in integrated circuit testing (100 μs to 10 ms). As a consequence, there is a sacrifice in voltage sensitivity and resolution, a tradeoff that can be improved by further optimization in the probe.

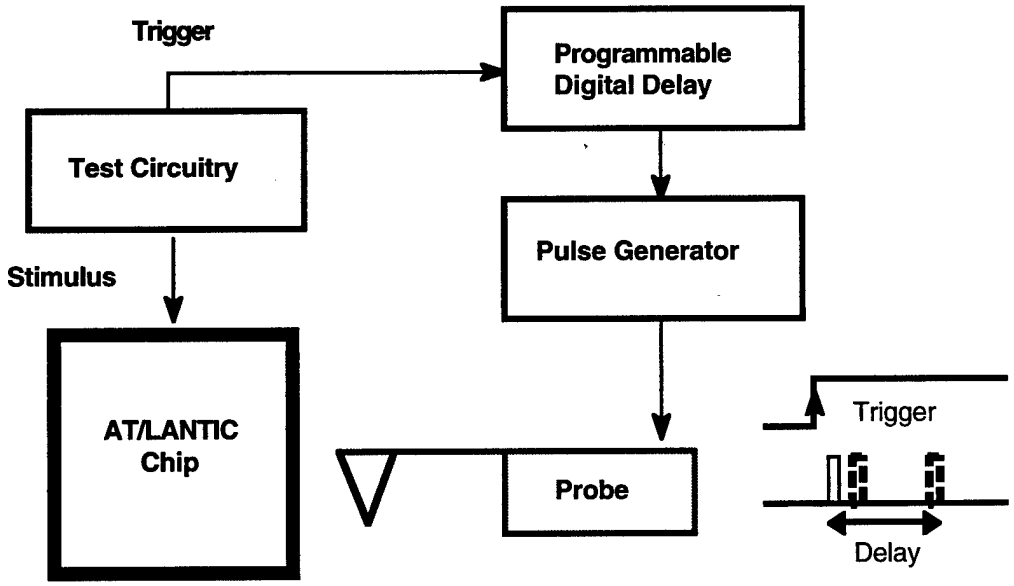


Figure 15. Experimental setup for measuring AT/LANTIC chip.

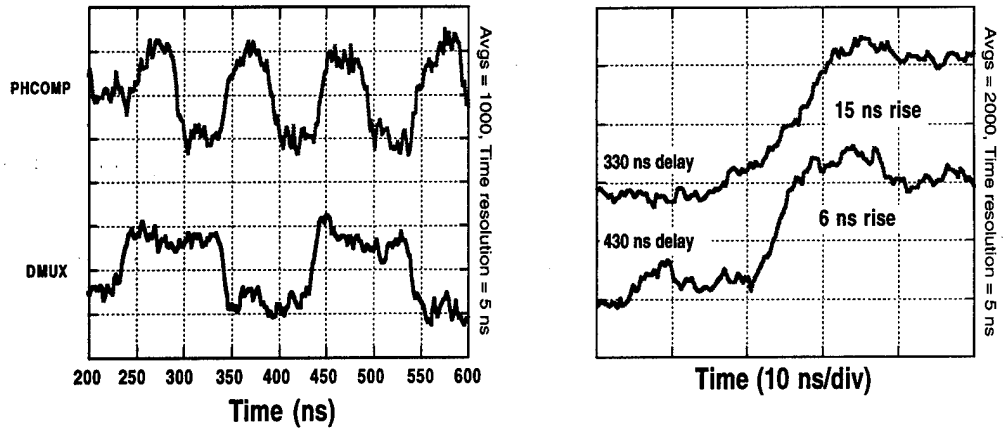


Figure 16. Measured data from the AT/LANTIC chip.

## 11. Custom High-Speed Cantilevers

The preceding experiments were all performed using gold-coated commercially available cantilevers, a scheme which will not work at frequencies greater than a few gigahertz due to parasitic impedances inherent in the cantilever itself. In order to obtain better temporal resolution, we microfabricated cantilevers with integrated transmission lines, based on the GaAs fabrication steps shown in Fig. 17.

First, a 0.5μm thick silicon nitride layer was deposited and etched, which formed the bulk of the flexible cantilever. Next, 1000 Å thin undergold metal was deposited, which made up the coplanar waveguide on the silicon nitride cantilever. This layer needed to be thin in order to prevent the curling of the cantilever due to thermal stresses. The thick overgold metal that followed formed the low loss coplanar waveguide on the substrate. The tips were evaporated using a Spindt tip process in which the photoresist hole closes off during evaporation to leave a sharp cone - tip after metal lift-off. Lastly, the GaAs substrate was etched out from under the AFM cantilever to free it. SEM images of the cantilever and the tip are shown in Figs. 18 and 19.

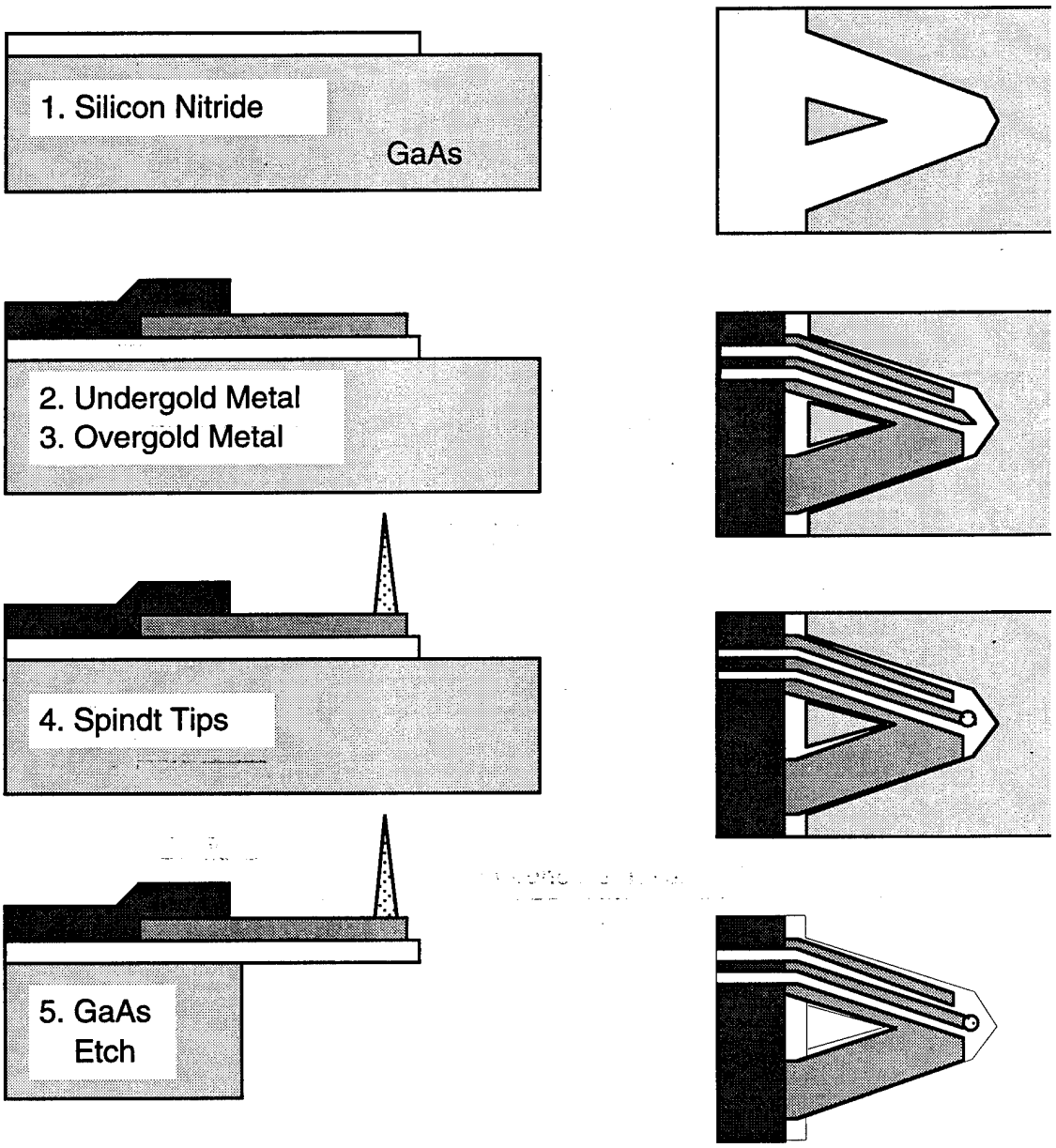


Figure 17. Fabrication steps for high-speed AFM cantilever.

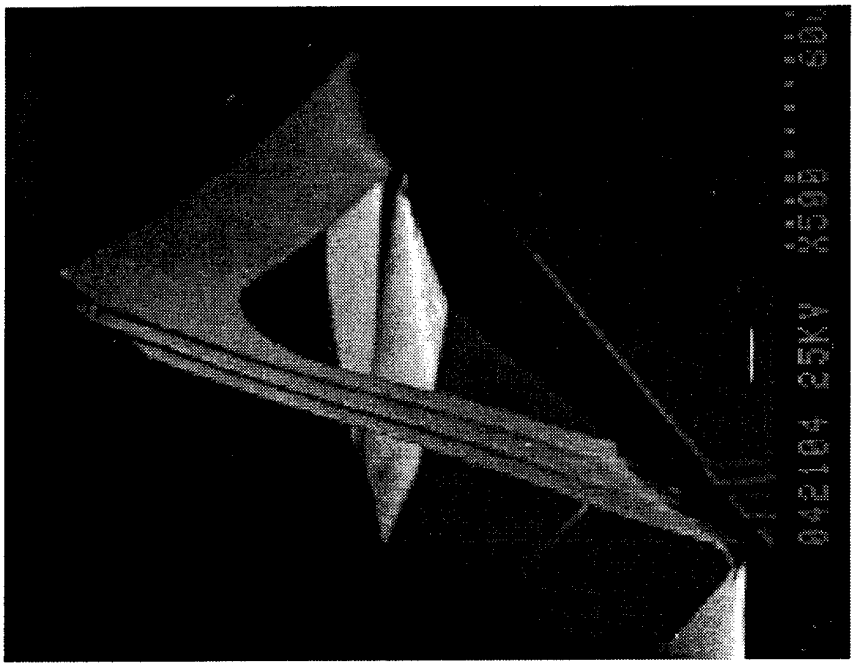

Figure 18. High-speed AFM cantilever.

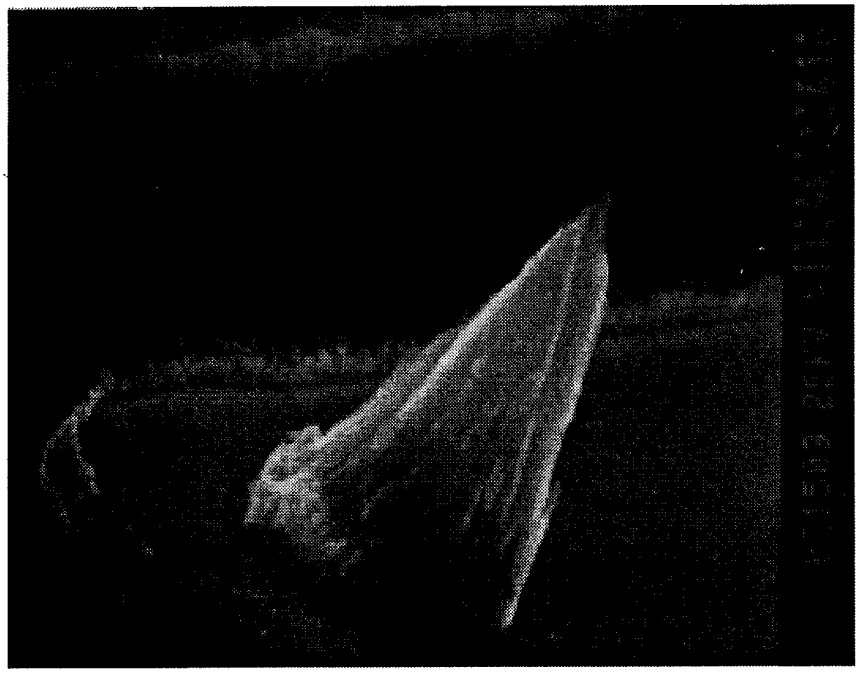

Figure 19. Close-up of Spindt tip.

Using this high-speed cantilever, we were able to observe voltage steps as short as 5 picoseconds on circuits, as shown in Fig. 20. In this experiment, we used nonlinear transmission line (NLTL) circuits, which can generate subpicosecond voltage steps [3], as both the source of the sampling signal to the tip and as the circuit under test. In the case of

the sampling signal, the integrated high speed cantilevers were wire-bonded to the output of one of the NLTLs. The NLTL circuits were driven with phase-locked synthesisers at 9 GHz and 9 GHz -1 kHz, generating an IF signal with harmonics of 1 kHz. Although equivalent-time sampling normally requires voltage pulses for the strobe signal, we were able to use voltage steps as the strobe signal by post-processing (numerically differentiating) the sampled signal. This avoids the problem of having to generate an impulse function from the NLTL step function. Furthermore, using the step function output directly improves the signal to noise ratio of the system since the sampling signal voltage is doubled upon reflection from the open transmission line.

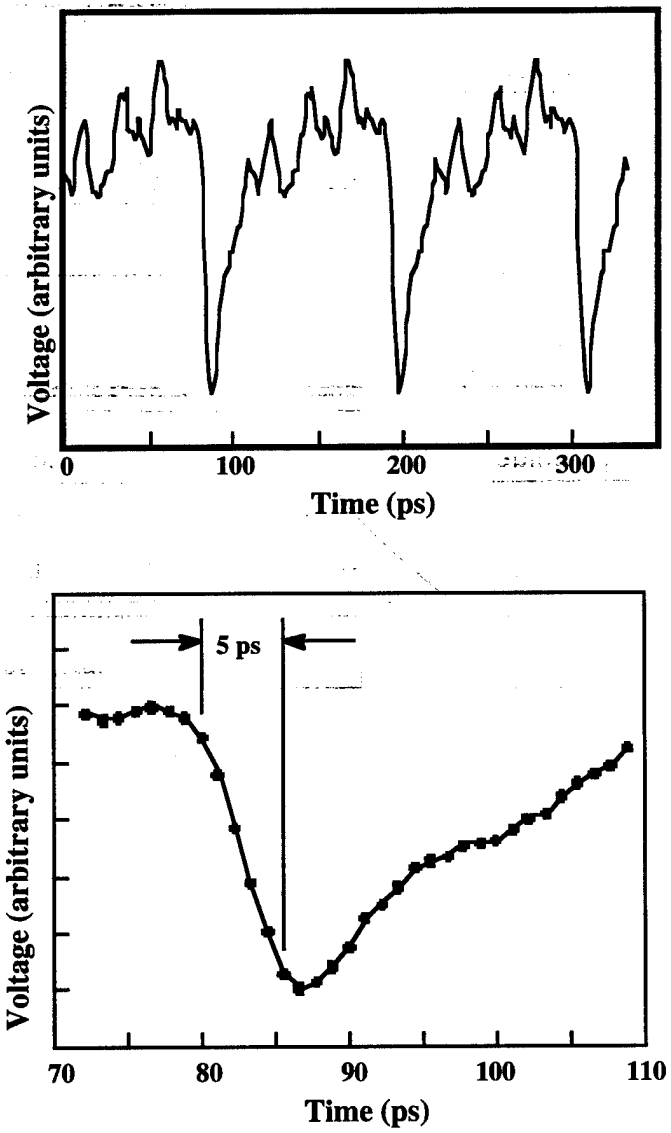


Figure 20. Measurements of a test NLTL with hybrid set-up.

## 12. Microwave Phase Measurements

One novel experiment that was done using the high-speed cantilevers involved the measurement of the phase change in the measured AFM deflection signal as a function of the applied phase shift to a microwave sinusoidal signal input into a coplanar waveguide. The experimental set-up is shown in Fig. 21. In this case, the reference signal for the lock-in amplifier was generated from the output of a mixer, mixing down the two source frequencies.

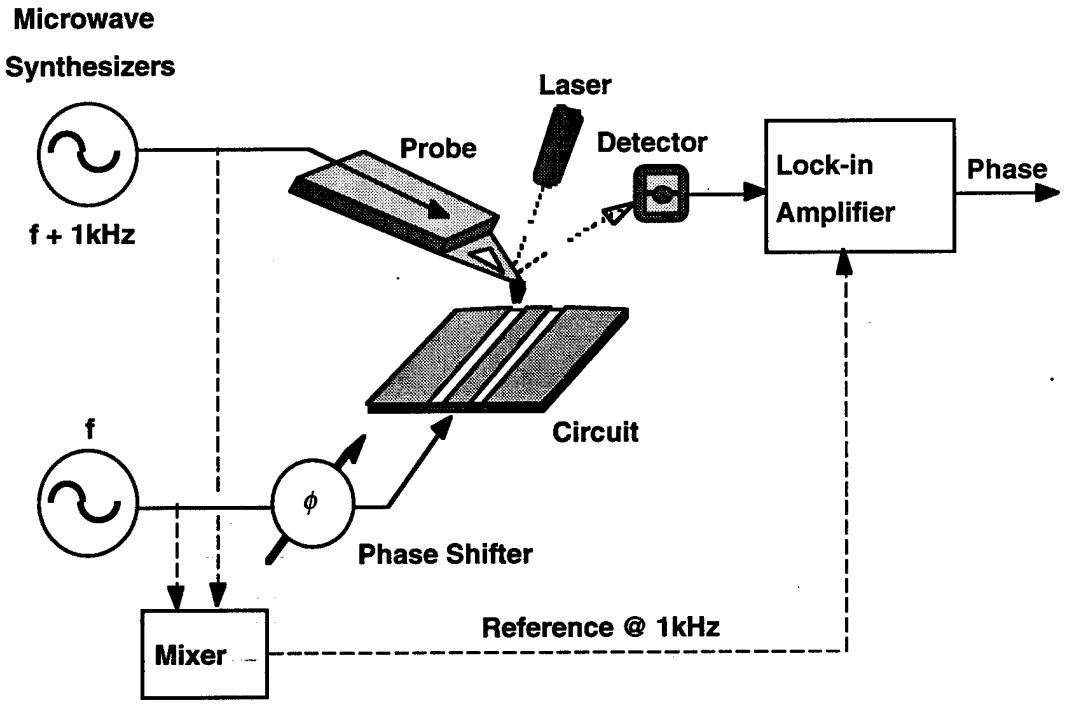


Figure 21. Experimental setup for microwave phase measurements.

The resulting phase measurements are shown in Fig. 22 for three different input frequencies. As can be seen from the plot, the measured phase shift is equal to the input phase shift. The slight variation at around 300 degrees is mainly due to the inaccuracies of the input phase shifter. Furthermore, the measured phase was quite stable in time, with only a 0.2 degree variation present over a 10 minute measurement window.

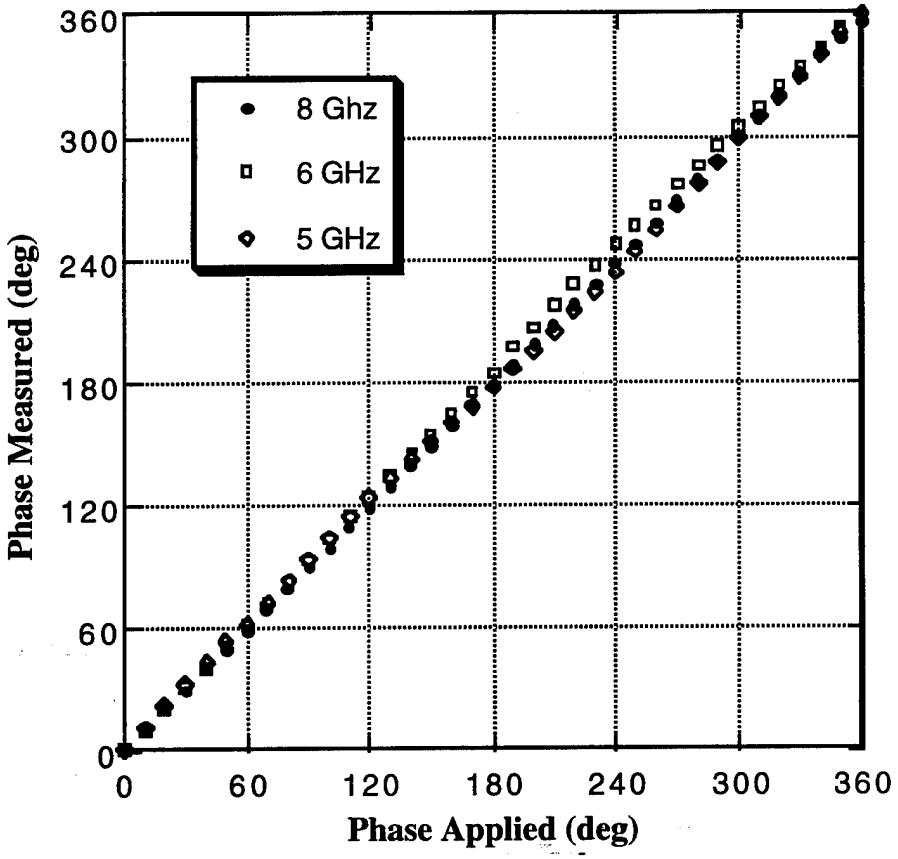


Figure 22. Microwave phase measurements at three input frequencies.

## 13. Integrated NLTL's and High-Speed Cantilevers

As described earlier, the time resolution achievable in the AFM voltage probe is determined largely by the speed of the signal that can be propagated to the tip. Since the NLTL circuit and the cantilever chip were wire-bonded together in the case of the hybrid approach of Section 11, the bandwidth of the sampling signal was limited by the wire bond parasitics. By integrating the NLTL circuit and the cantilever on the same substrate, we anticipated that these parasitics could be avoided, allowing us to obtain sub-picosecond time resolution. This improved time resolution would then allow for the measurement of carrier transport effects in high speed electrical and opto-electronic devices.

The process flow for this monolithic integration is shown in Fig. 23. This process is novel in that it is one of the first to combine monolithic microwave integrated circuit (MMIC) processing technology with micromachining techniques. It involves ten mask steps. Of these, the ohmic metal (Step 1), diode etch (Step 2), isolation (Step 3) Schottky metal (Step 4) and interconnect metal (Step 6) involve the fabrication of the NLTL circuits. The high-speed cantilever fabrication is similar to that described in the previous section, except that a two metalization-level "quasi-stripline" waveguide design was used which improved impedance matching at the GaAs / nitride cantilever interface.

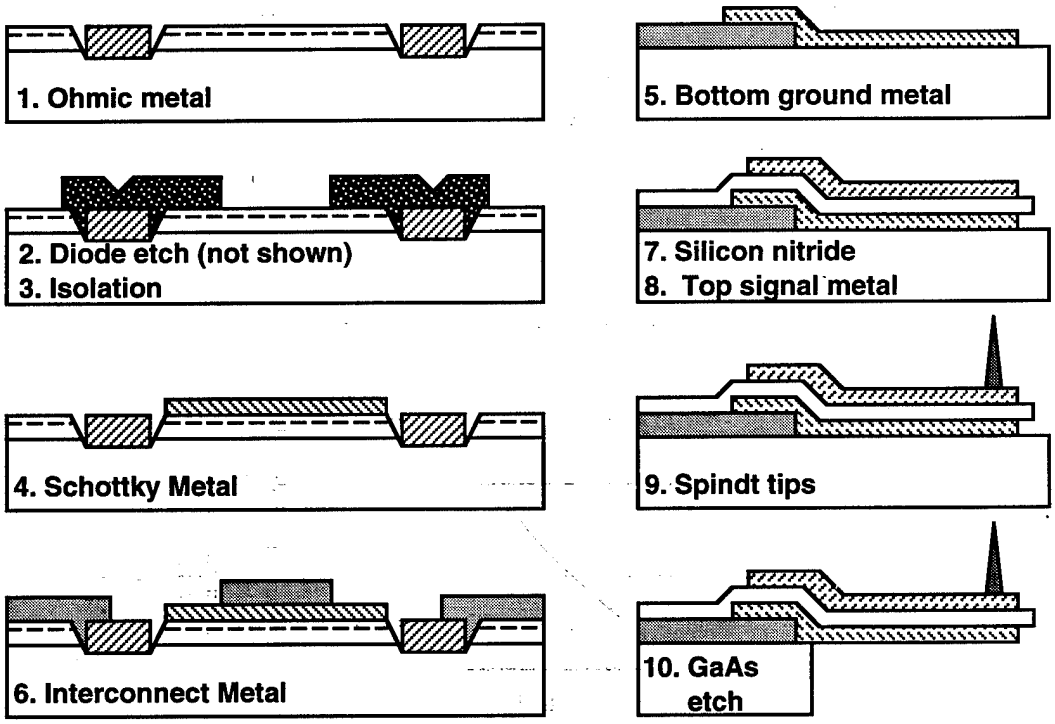


Figure 23. Process flow for integrated NLTLs and high-speed AFM cantilevers.

The resulting integrated NLTLs and high-speed cantilevers (NLTL/CLs) are shown in Figs. 24 to 26. Figure 24 shows a photo of the end of the NLTL circuit terminating in a high-speed cantilever. Figure 25 shows photos of several variations of high-speed cantilever designs. Figure 26 shows an SEM photo of an improved Spindt tip, which uses two levels of photoresist to allow for taller tips and higher aspect ratios.

The epitaxial and layout design for the NLTLs used in this project were adapted from designs of Dr. Dan Van Der Weide [3] who was able to obtain measurements of 480 fs voltage transients using these NLTL circuit designs.

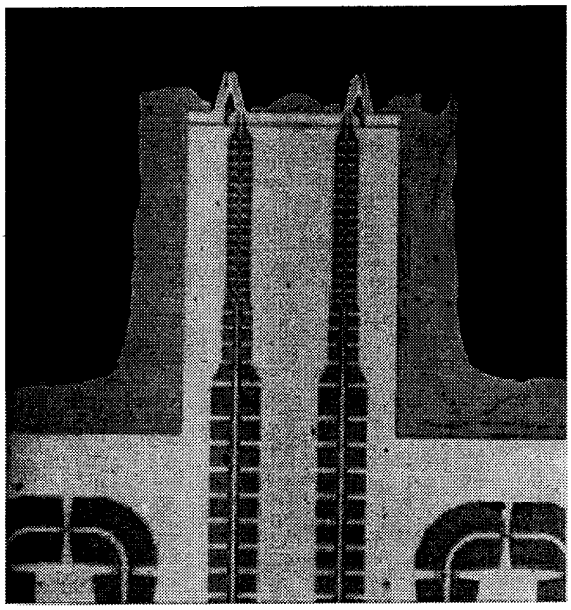

Figure 24. Fabricated NLTL/CL.

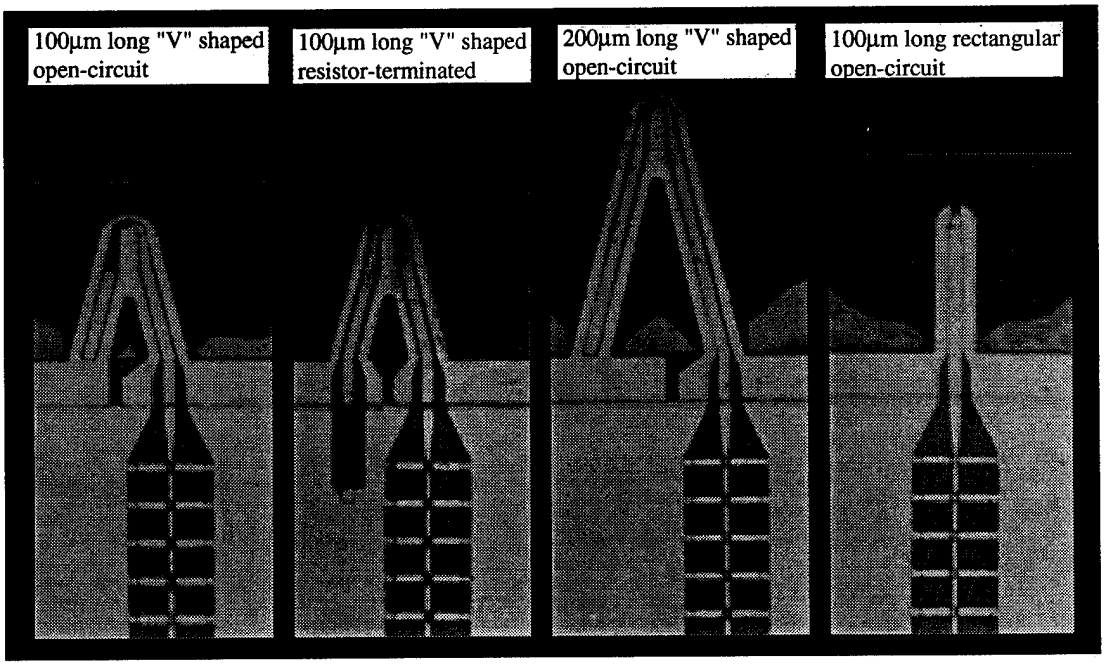


Figure 25. High-speed AFM cantilevers on fabricated NLTL/CLs.

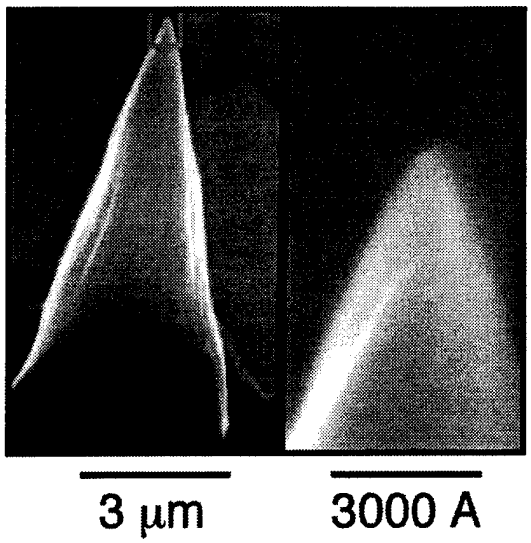


Figure 26. Fabricated two-level resist Spindt-tips.

Using these NLTL/CL probes, equivalent-time sampling measurements were done on a test NLTL circuit using the set-up shown in Fig. 27. Here, two separate high-frequency sources were used to drive the NLTLs of the sample and probe. The frequencies

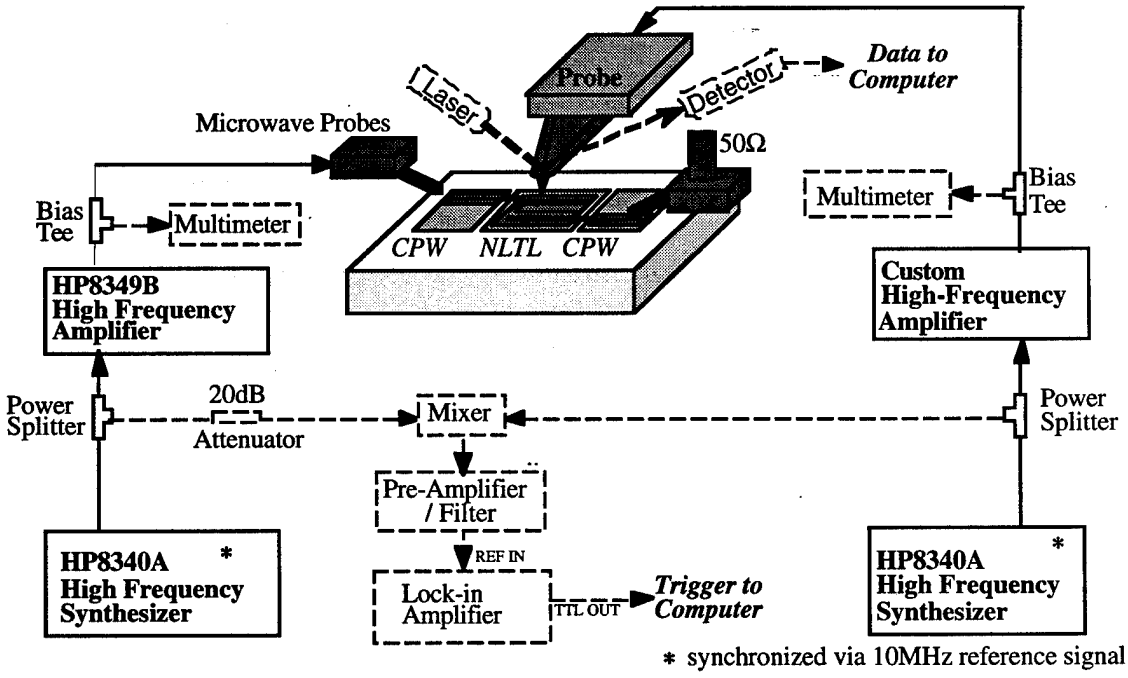


Figure 27. Experimental setup for equivalent time sampling measurement.

were offset from each other by 500 Hz, with a trigger for the data analysis being mixed down to this frequency from the two source frequencies in order to minimize phase jitter. The output of the position sensitive detector was signal-averaged and then differentiated in time, in order to compensate for the fact that the probe signal was a sawtooth as opposed to a pulse function (as described in Section 11). The fastest results obtained are shown in Fig. 28, revealing a measured falltime as fast as 1 picosecond. This is the fastest voltage signal ever measured using a Scanning Probe Microscope.

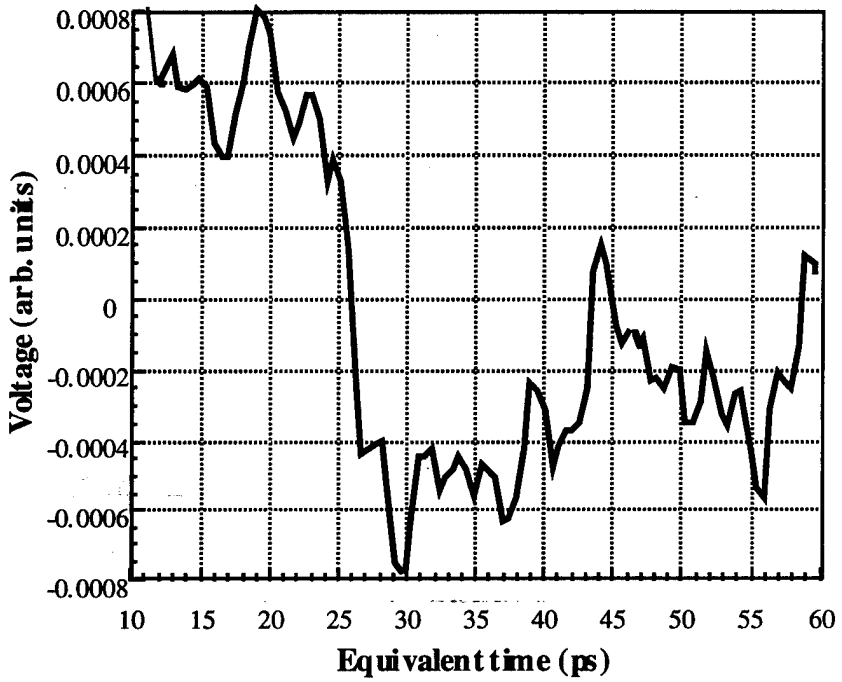


Figure 28. Equivalent-time sampling signal showing 1 ps falltime.

Harmonic mixing data was also taken using this set-up, by simply feeding the output of the position-sensitive detector into a spectrum analyser and vector-averaging. The results are shown in Fig. 29, which show a measured equivalent-frequency as high as 333 GHz. Again, this is the highest frequency measured by an SPM probe.

All of these measurements were done using an open-circuit terminated high-speed cantilever. Though this cantilever was able to generate the fastest measured voltage transients, it nevertheless included voltage reflection effects due to the reflection of the entire NLTL signal off of the open end back into the NLTL circuit. In order to reduce these reflection effects, a resistive terminated cantilever was designed and fabricated which would terminate the NLTL signal so that it would not reflect back into the circuit. However, when

this probe was tested, a large thermally induced background signal overwhelmed the desired electric force signal.

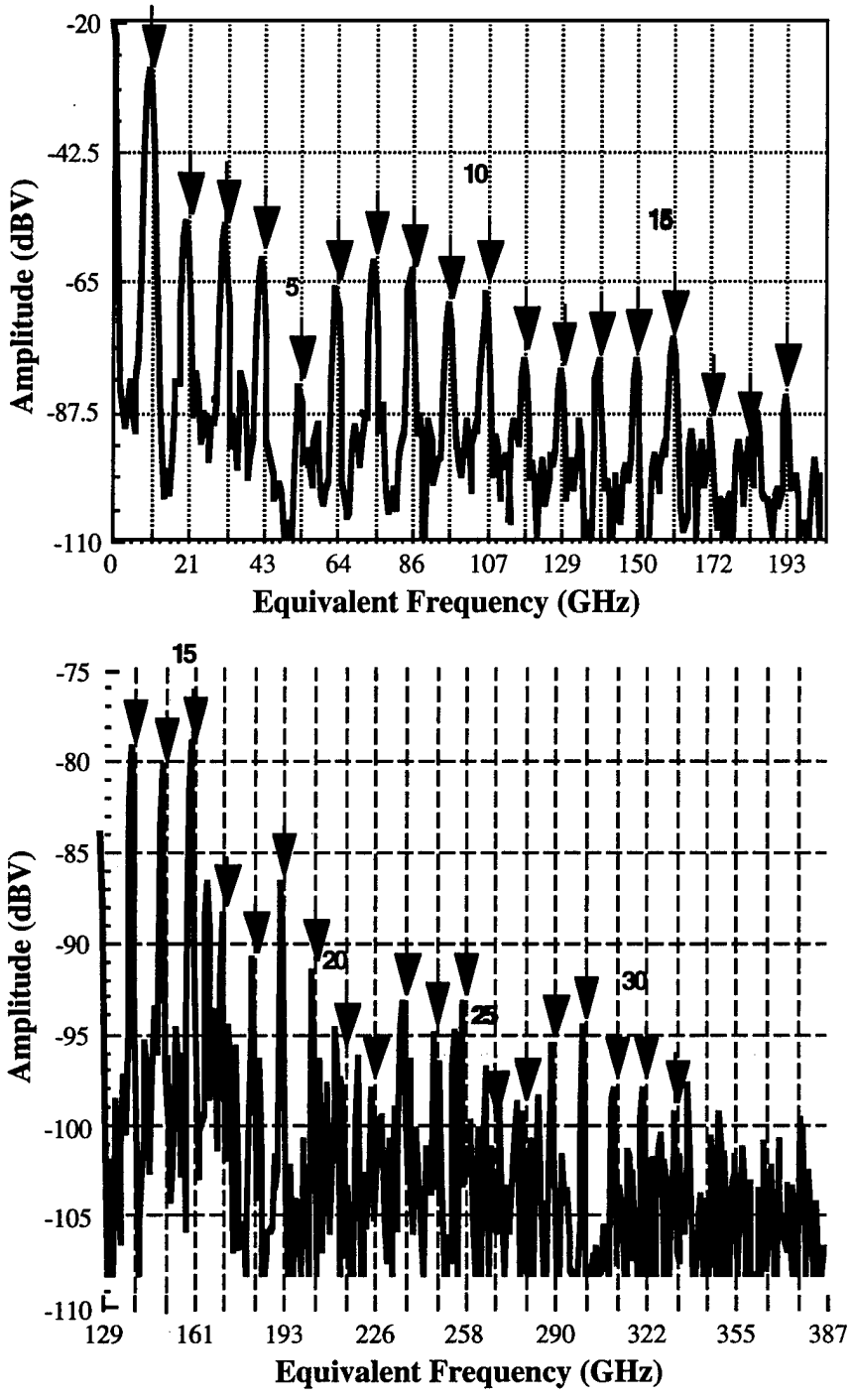


Figure 29. Harmonic mixing measurements.

## 14. Scanning Electrical Contact Sampler

Another method of making nanometer-scale ultrafast voltage measurements with a scanning probe microscope involves operating the AFM in contact mode and using Schottky diodes as mixers.

A simple description of the theory behind this contact sampler is that the SFM tip makes contact with the conductive sample-under-test that generates a fast RF signal which is to be measured. This signal is then carried down the conductive cantilever to a pair of fast sampling diodes that are periodically pulsed on with an external LO (local oscillator) signal. This LO signal is offset from the RF signal by a known offset frequency called the intermediate frequency (IF). The output of the diodes is low-pass-filtered to generate an output IF signal which is essentially a time-expanded version of the measured RF signal.

This system uses the same equivalent-time sampling concepts described earlier in this report. The difference is that, instead of making use of inherent nonlinearities in the AFM electric force, it is the sampling diodes which perform the nonlinear mixing of the LO pulses with the measured RF signal. It is, therefore, largely the speed of these sampling diodes and LO signal source as well as the parasitics associated with the signal path from the tip to these sampling diodes which determine the system measurement bandwidth. Also, an external low-pass-filter circuit is needed to then generate the low-frequency IF output whereas, in the AFM Voltage Probe case, it is the cantilever response itself which accomplishes the low-pass filtering.

The schematic diagram of the scanning electrical sampler used for this experiment is shown in Fig. 30. The scanning electrical sampler itself is drawn within the dashed lines. SD are the Schottky diodes used in the sampling switches. $C_h$ are hold capacitors which charge up to the device-under-test (DUT) voltage, $V_{RF}$, when the diodes are conducting. The DUT has an output impedance $R_s$, and its ground is connected to the ground of the sampler through a connection that has parasitic inductance L. $R_{IF}$ provide dc bias for the diodes, and also couple the hold capacitors to the IF preamplifier. $R_g$ are resistors that couple the hold capacitors to ground. $C_i$ are input coupling capacitors that serve to ac-couple the sampler circuit to the LO pulse inputs. The LO pulses, supplied by step-recovery diodes (not shown), are 136 ps in pulse width and 4.8 V in amplitude. One LO pulse is a negative going pulse, the other is a positive-going pulse, and the two are synchronised. The IF preamplifier is a low-noise, high-impedance amplifier. Table 2 lists the component specifications for a design with RF fundamental frequency, f, of 100 MHz, and an IF frequency, $\Delta f$, of 7 Hz.

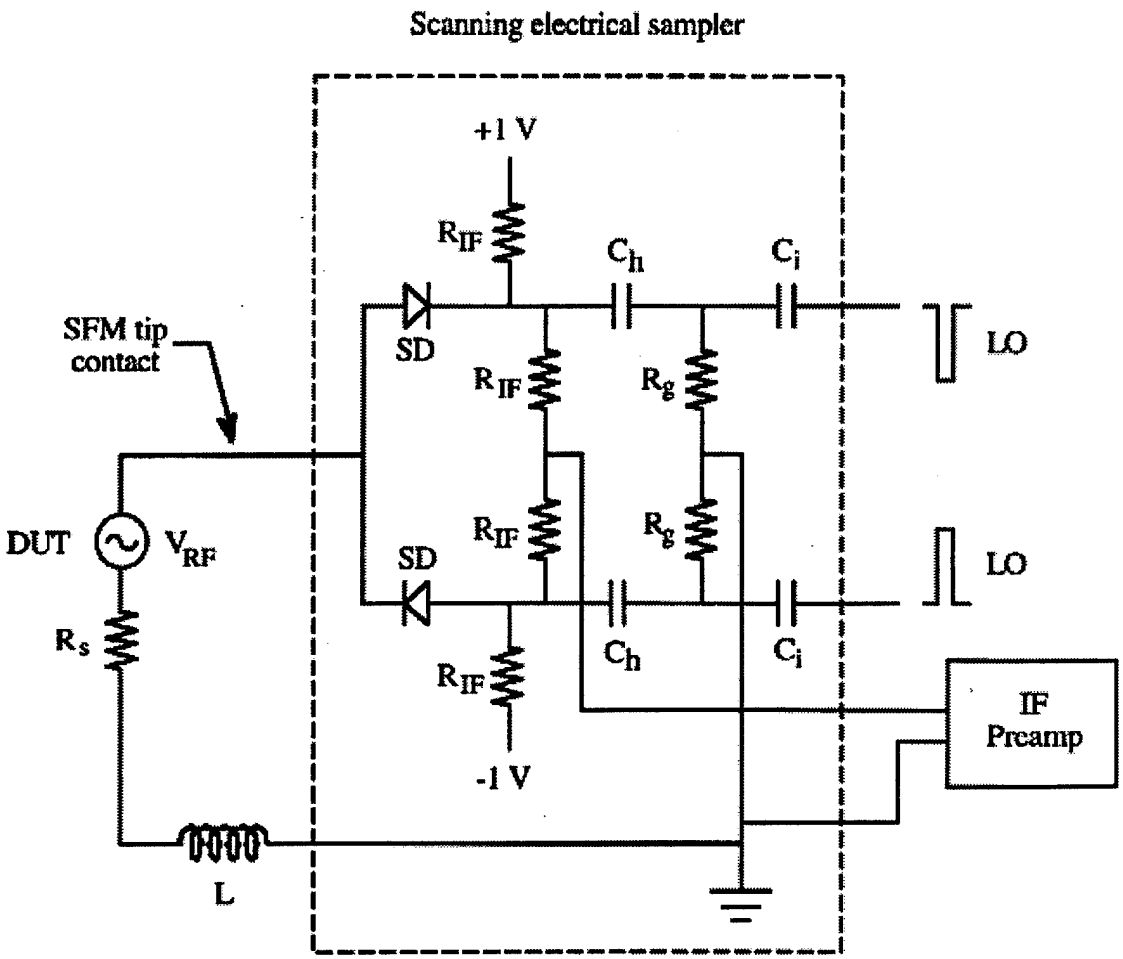


Figure 30. Schematic diagram of the scanning electrical sampler.

**Table 2 - Circuit Specifications for Scanning Electrical Sampler**

| | |
|---|---|
| $R_g$ | 510 Ω |
| $R_{IF}$ | 2.2 MΩ |
| Ch | 1 pF |
| Ci | 1 nF |
| L | ≈ 2 μH |
| Preamp input resistance | 100 MΩ |
| Preamp input capacitance | 25 pF |
| Preamp input cable capacitance | 200 pF |

A prototype scanning electrical sampler was constructed based on this design, using surface mounted components and a commercially purchased SFM cantilever sputter coated with several hundred Ångstroms of gold. Using this probe, proof of principle experiments were performed with an experimental set-up as shown in Fig. 31. Here, step-recovery diodes generate ~100 ps pulses for both the LO sampling source and the DUT RF signal. The DUT was a through-line CPW fabricated on an alumina substrate. Two phase-locked synthesizers were used as sources, with the RF source frequency set to 100 MHz. The RF pulses were also sent through a 20 dB attenuator to keep from overloading the sampler. The output of the DUT CPW was fed to a sampling scope for comparison with the probe measurement.

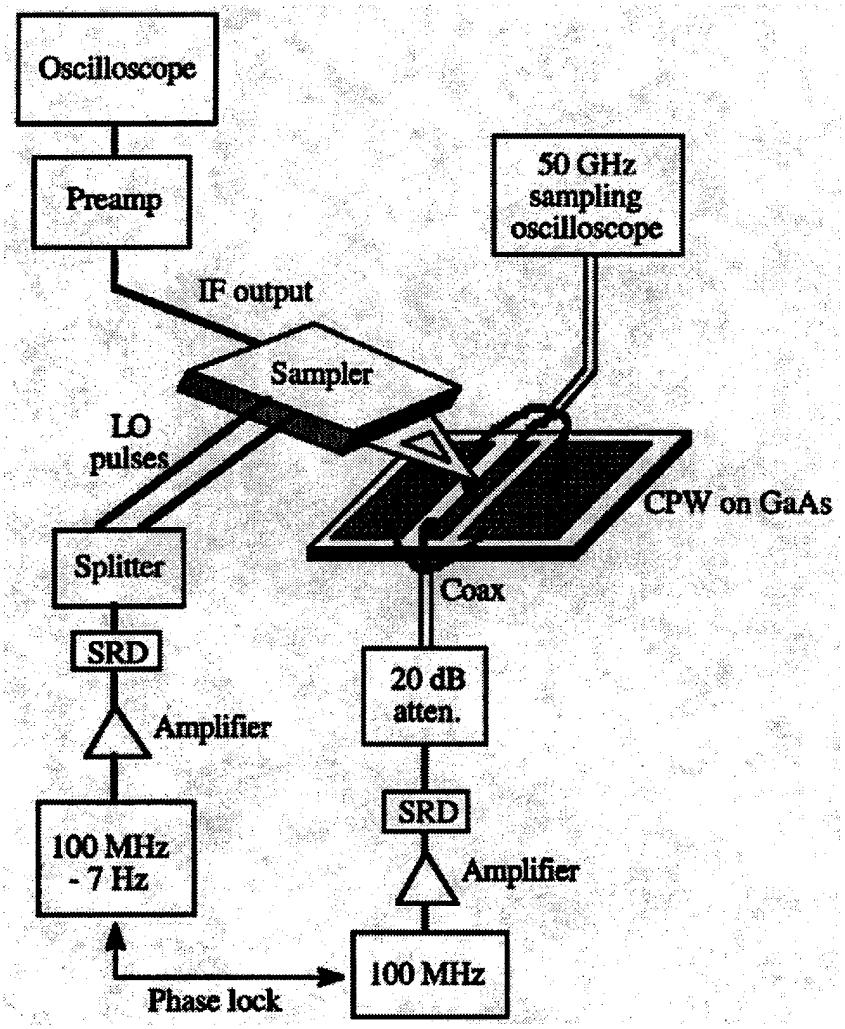


Figure 31. Experimental setup for characterization of the scanning electrical sampler.

The resulting measurements for both the scanning electrical contact sampler and the sampling scope are shown in Fig. 32, where the longer pulse width in the case of the scanning electrical contact sampler measurement is largely due to it being determined by the convolution of the RF signal with the LO signal.

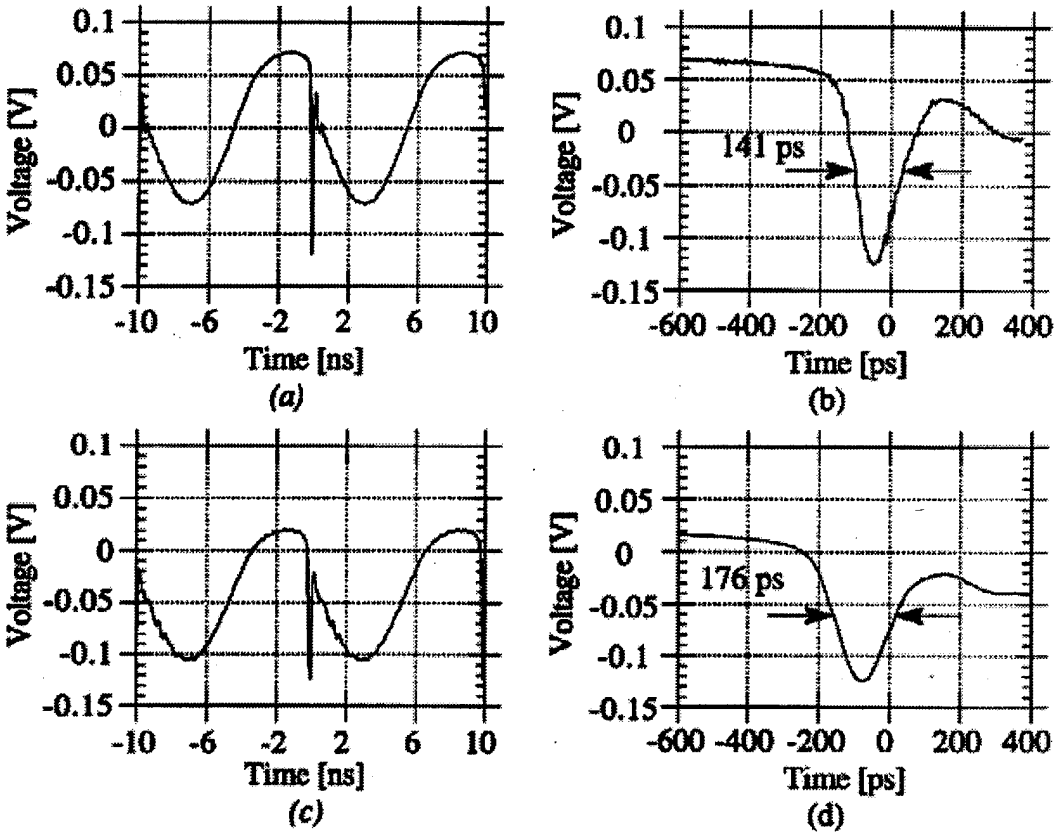


Figure 32. Measurements of SRD pulse using a sampling oscilloscope (a and b) and the scanning electrical sampler (c and d).

Lastly, as was expected, the voltage noise performance was much better than that for the AFM voltage probe. Theoretical predictions for this contact sampler gave noise voltages at low frequencies on the IF output of 130 nV / $\sqrt{Hz}$. The actual measured noise level was higher than the theoretical level at low frequencies, but dropped below that level at frequencies above ~ 4 kHz.

## 15. Piezoresistive Gallium Arsenide Cantilever

One of the critical elements of a scanning force microscope is the deflection sensor which measures the displacement of the cantilever. The optical deflection sensing technique is the one most commonly used today. However, there are circumstances in which one would wish to be able to acquire an image by scanning the SFM tip across a sample as opposed to scanning the sample itself, as with the measurement of electrical devices with rigid coaxial cables or microwave probes attached. In this case, the optical lever method makes it difficult to scan the tip, since one must then resort to complex mechanical and optical designs to keep the optical beam aligned on the cantilever.

Piezoresistive deflection sensing offers an attractive alternative. It works by sensing the change in resistance of a resistor fabricated on a piezoresistive SFM cantilever. The piezoresistance of the material of the SFM cantilever, a novel GaAs/AlGaAs epi structure in this case, gives rise to a change in the material resistivity when the cantilever is stressed - as is the case with cantilever deflection. Therefore, the measured resistance is a known function of the materials piezoresistive behavior and the cantilever deflection.

For a cantilever configuration as shown in Fig. 33, the fractional change in resistivity can be calculated to be:

$$\frac{\Delta R}{R} = \frac{6\Pi_l}{wt^2} F \qquad (21)$$

where $\Pi_l$ is the effective longitudinal piezoresistive coefficient, w and t are the width and thickness of the cantilever, and F is the applied force. Confining the piezoresistor to the end of the cantilever, as in this configuration, helps to increase its response. The change in resistance of the piezoresistor can then be measured with a Wheatstone bridge.

A schematic drawing of a fabricated cantilever is shown in Fig. 34. In this design, one leg at the base of the cantilever serves as the piezoresistor while the other is simply used as a mechanical support.

To measure the piezoresistive cantilever performance, the change in the piezo-resistance was monitored while the cantilever was deflected by a piezo-controlled STM tip in contact with the cantilever. From these measurements, the effective longitudinal piezoresistive coefficient was calculated as $3.0 \times 10^{-9}$ $m^2/N$. This is in fair agreement with the value of $2.4 \times 10^{-9} m^2/N$ found in the literature.

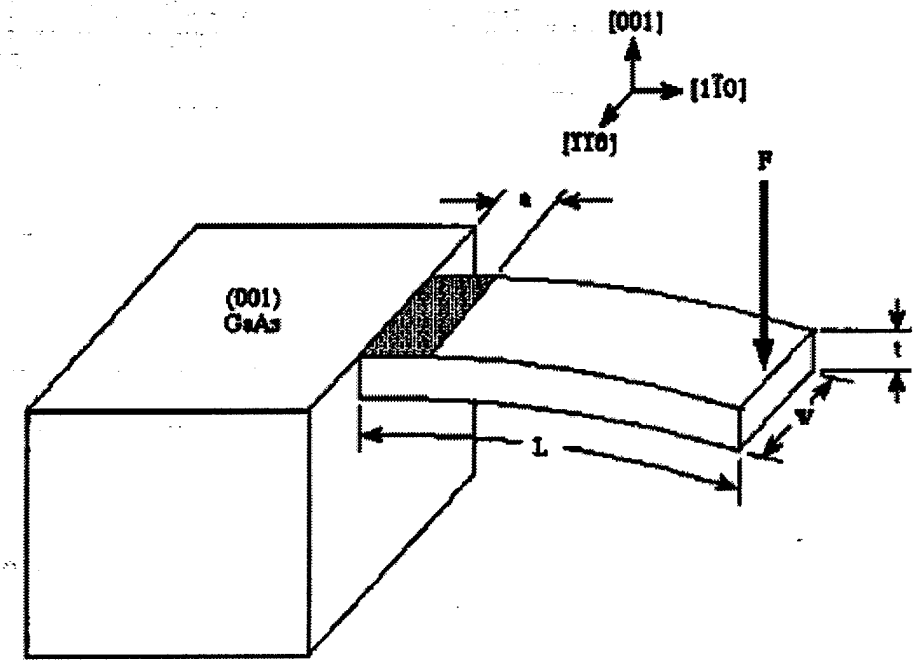


Figure 33. Schematic diagram of piezoresistive cantilever.

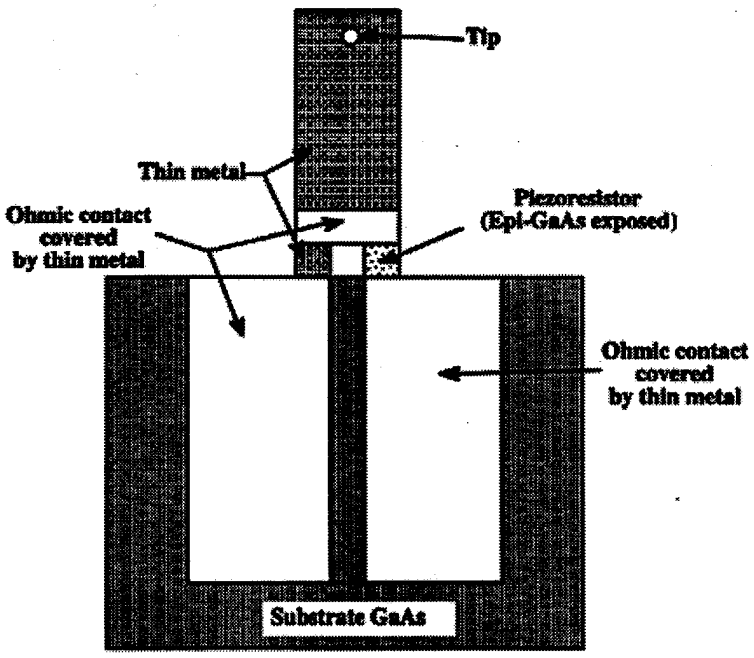


Figure 34. Schematic drawing of a fabricated cantilever.

## 16. Suggestions for Further Reading

This final report excluded many of the details behind the numerous projects mentionned above. For further information, the reader can refer to the Ph.D. theses of the various students involved in this project. These are listed below according section/project:

| Section | | Students Involved |
|---|---|---|
| **Theory:** | | |
| 4. | High-frequency electric force measurements with an AFM voltage probe | Sam Hou, Francis Ho, and Bettina Nechay |
| 5. | Ultimate time resolution | Sam Hou |
| 6. | Voltage resolution | Sam Hou and Francis Ho |
| 7. | Lateral Resolution | Sam Hou and Francis Ho |
| **Experiments:** | | |
| 8. | Early Proof-of-Principle Experiments | Sam Hou and Francis Ho |
| 9. | Probe Design and Engineering | Sam Hou |
| 10. | Measurements of Integrated Circuits | Francis Ho and Sam Hou |
| 11. | Custom High-speed Cantilevers | Sam Hou, Bettina Nechay, and Francis Ho |
| 12. | Microwave Phase Measurements | Bettina Nechay |
| 13. | Integrated NLTL's and high-speed cantilevers | Bettina Nechay |
| 14. | Scanning Electrical Contact Sample | Francis Ho |
| 15. | Piezoresistive Gallium Arsenide Cantilever | Francis Ho |

## References


[1] J. T. L. Thong, ed., *Electron Beam Testing Technology - Microdevices, Physics and Fabrication Technologies*(Plenum Press, New York, 1993).

[2] C. J. Madden, R. A. Marsland, M. J. W. Rodwell, D. M. Bloom, and Y. C. Pao, "Hyperabrupt-Doped GaAs Nonlinear Transmission Line for Picosecond Shock-Wave Generation," *Appl. Phys. Lett.* **54**, 1019-1021 (March 1989).

[3] D.W. van der Weide, "Delta-Doped Schottky Diode Nonlinear Ttransmission Lines for 480-fs, 3.5-V Transients," *Appl. Phys. Lett.* **65**, 881-883 (August 1994).

[4] G. Binnig and H. Rohrer, "Scanning Tunneling Microscopy," *Helvetica Physica Acta*, **55**, 726 (1982).

[5] G. Binnig, C. F. Quate, and Ch. Gerber, "Atomic Force Microscope," *Phys. Rev. Lett.* **56**, 930 (1986).